

1 **Enzymatic and spectroscopic properties of a thermostable [NiFe]-**
2 **hydrogenase performing H₂-driven NAD⁺-reduction in the presence of O₂**

3 Janina Preissler ^{[a],1}, Stefan Wahlefeld ^{[a],1}, Christian Lorent ^[a], Christian Teutloff^[b], Marius
4 Horch ^{[a]*}, Lars Lauterbach ^{[a]*}, Stephen P. Cramer ^[c], Ingo Zebger^{[a]*}, and Oliver Lenz^{[a]*}

5 ^[a] Technische Universität Berlin, Institut für Chemie, Sekr. PC14, Straße des 17. Juni 135, D-
6 10623 Berlin (Germany)

7 ^[b] Freie Universität Berlin, Fachbereich Physik, Arnimallee 14, D-14195 Berlin, (Germany)

8 ^[c] University of California, Department of Chemistry, One Shields Ave, Davis, CA 95616
9 (USA).

10
11 ¹ These authors contributed equally to the study

12 * Corresponding authors

13
14
15 **KEYWORDS**

16 Hydrogenase; hydrogen; oxyhydrogen reaction; nickel; iron; respiratory Complex I, flavin;
17 iron-sulfur cluster; pyridine nucleotide; enzyme kinetics; infrared vibrational spectroscopy,
18 electron paramagnetic resonance spectroscopy; nuclear resonance vibrational spectroscopy;
19 biotechnology; cofactor recycling

21 ABSTRACT

22 Biocatalysts that mediate the H₂-dependent reduction of NAD⁺ to NADH are attractive from
23 both a fundamental and applied perspective. Here we present the first biochemical and
24 spectroscopic characterization of an NAD⁺-reducing [NiFe]-hydrogenase that sustains
25 catalytic activity at high temperatures and in the presence of O₂, which usually acts as an
26 inhibitor. We isolated and sequenced the four structural genes, *hoxFUYH*, encoding the
27 soluble NAD⁺-reducing [NiFe]-hydrogenase (SH) from the thermophilic betaproteobacterium,
28 *Hydrogenophilus thermoluteolus* TH-1^T (*Ht*). The *Ht*SH was recombinantly overproduced in
29 a hydrogenase-free mutant of the well-studied, H₂-oxidizing betaproteobacterium *Ralstonia*
30 *eutropha* H16 (*Re*). The enzyme was purified and characterized with various biochemical and
31 spectroscopic techniques. Highest H₂-mediated NAD⁺ reduction activity was observed at
32 80 °C and pH 6.5, and catalytic activity was found to be sustained at low O₂ concentrations.
33 Infrared spectroscopic analyses revealed a spectral pattern for as-isolated *Ht*SH that is
34 remarkably different from those of the closely related *Re*SH and other [NiFe]-hydrogenases.
35 This indicates an unusual configuration of the oxidized catalytic center in *Ht*SH.
36 Complementary electron paramagnetic resonance spectroscopic analyses revealed spectral
37 signatures similar to related NAD⁺-reducing [NiFe]-hydrogenases. This study lays the
38 groundwork for structural and functional analyses of the *Ht*SH as well as application of this
39 enzyme for H₂-driven cofactor recycling under oxic conditions at elevated temperatures.

40

41 INTRODUCTION

42 Enzymatic oxidation of dihydrogen (H₂) is a widespread trait in the microbial world and is
43 used by many microbes to gain metabolic energy [1,2]. The reversible cleavage of H₂ into
44 protons and electrons is mediated by complex metalloenzymes designated as hydrogenases
45 [3]. In particular, the coupling of H₂ oxidation with aerobic respiration, i.e. the controlled

46 Knallgas reaction ($\text{H}_2 + \frac{1}{2} \text{O}_2 \rightarrow \text{H}_2\text{O}$), releases a high yield of free energy of $\Delta G^\circ = -237.2$
47 kJ per mol of H_2 . Aerobic H_2 oxidation, however, requires hydrogenases that withstand the
48 toxic effect of O_2 . Among the different hydrogenase types, there is only one subclass that
49 sustains H_2 oxidation in the presence O_2 , namely the O_2 -tolerant [NiFe]-hydrogenases [4].
50 One prominent member is the soluble NAD^+ -reducing [NiFe]-hydrogenase (SH) from the
51 betaproteobacterium *Ralstonia eutropha* H16 (*Re*), which is a well-known Knallgas
52 bacterium possessing an H_2 -driven chemolithoautotrophic metabolism [5]. *ReSH* directly
53 couples H_2 oxidation with the reduction of NAD^+ , thereby producing NADH, which is used
54 both for energy conservation (through Complex I and the respiratory chain) and for CO_2
55 fixation *via* the Calvin cycle.

56 The *ReSH* is a bi-modular enzyme consisting of four essential subunits, HoxFUYH, that
57 harbor the [NiFe] active site, where H_2 conversion takes place, and the catalytic center for
58 NAD^+ reduction, which carries a flavin mononucleotide (FMN) [6]. Electron transfer
59 between the two active sites is mediated by four [4Fe4S] clusters and one [2Fe2S] site.
60 Another FMN group has been suggested to be located close to the [NiFe] active site [7]. Two
61 copies of the non-essential HoxI protein, whose function remains so far elusive, are also
62 integral part of the *ReSH* [8]. The overall subunit composition as well as the cofactor
63 arrangement of NAD^+ -reducing [NiFe]-hydrogenases are reminiscent of the situation in the
64 peripheral arm of Complex I. In fact, it is anticipated that the SH represents a phylogenetic
65 ancestor of Complex I [9,10], for which crystal structures are available [11]. Unfortunately,
66 the *ReSH* has so far defied crystallization.

67 Three of four highly conserved cysteines coordinating the [NiFe] active site metal ions in the
68 HoxH subunit are missing in the homologous subunit of Complex I (Nqo4 in case of *Thermus*
69 *thermophilus*). According to amino acid sequence comparisons and numerous spectroscopic
70 studies, the *ReSH* carries a [NiFe] center similar to that of canonical [NiFe]-hydrogenases

71 [6,12,13]. Two of the four conserved cysteines serve as terminal nickel ligands, while the
72 remaining two coordinate both the nickel and the iron ions. The iron is further equipped with
73 one carbon monoxide and two cyanide ligands, which are supposed to maintain a low-spin
74 Fe^{II} state throughout the catalytic cycle. The nickel ion, however, changes its redox state
75 during H₂/H⁺ turnover [6]. As the *ReSH* is catalytically active under aerobic conditions, a
76 contact of the active site with O₂ is a very likely event. Nonetheless, the H₂ turnover rate
77 remains at almost 100 % even in the presence of 20 % O₂, which makes *ReSH* the “world
78 record holder” among O₂-tolerant, energy-converting [NiFe]-hydrogenases [14,15]. Moreover,
79 the *ReSH* represents the first hydrogenase, for which a catalytic conversion of O₂ into water
80 has been demonstrated [15]. The exceptional O₂ tolerance and the high turnover rates of the
81 *ReSH* attracted scientists to employ the enzyme both *in vitro* and *in vivo* for H₂-driven
82 NAD(P)H cofactor regeneration in biotechnologically relevant applications [16–19]. Though
83 very efficient in NADH recycling, however, the *ReSH* has the disadvantage of being
84 temperature-sensitive [20]. Both the lack of a crystal structure of an NAD(P)⁺-reducing
85 [NiFe]-hydrogenase and the limited temperature stability of *ReSH* have prompted us to seek
86 out a thermostable version of this enzyme.

87 *Hydrogenophilus thermoluteolus* TH-1^T (*Ht*) has been described as an aerobic, facultatively
88 chemolithoautotrophic, hydrogen-oxidizing microorganism, which – like *R. eutropha* –
89 belongs to the phylogenetic class of betaproteobacteria [21]. It shows optimal
90 chemolithoautotrophic growth with a H₂:O₂:CO₂ gas mixture of 7:2:1 at a temperature of
91 52 °C [22]. This suggests the presence of at least one O₂-tolerant [NiFe]-hydrogenase. Indeed,
92 a recent study confirmed the presence of an SH-like enzyme in the moderate thermophile [23].
93 However, neither the corresponding genetic information nor a physiological or spectroscopic
94 characterization of the *HtSH* is so far available.

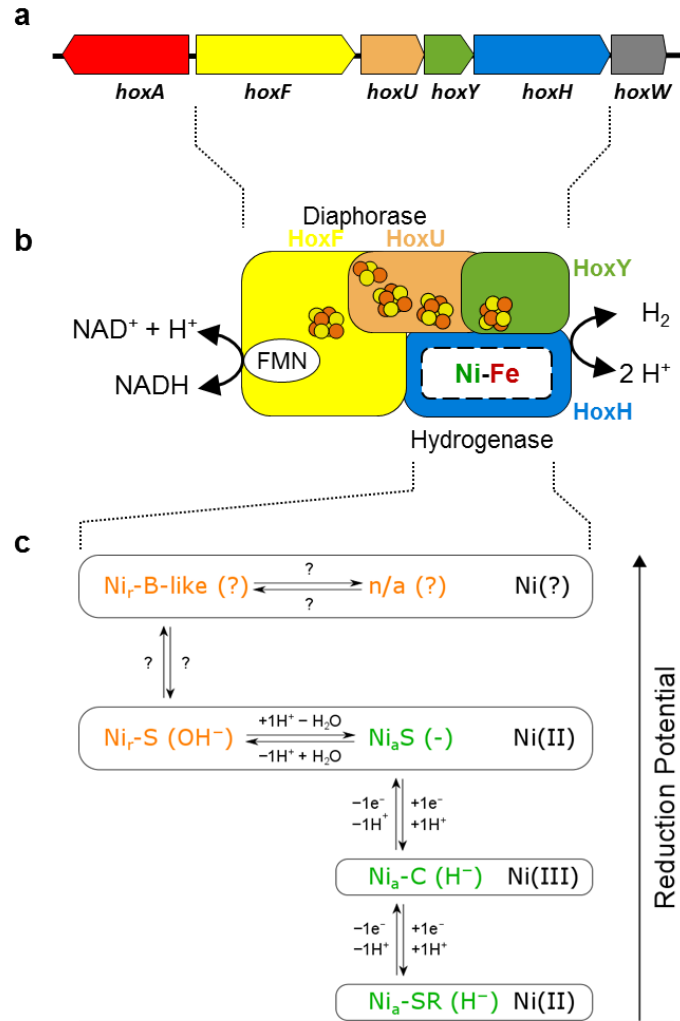
95 In this study, we present the DNA sequence of the structural genes of the four *HtSH* subunits
96 in addition to the gene encoding the *HtSH*-specific endopeptidase. The *HtSH* was
97 recombinantly overproduced in *R. eutropha* and – upon purification – characterized by means
98 of biochemical and spectroscopic methods. It turned out to be the first characterized [NiFe]-
99 hydrogenase that performs H₂-driven NAD⁺ reduction at elevated temperatures and in the
100 presence of O₂.

101

102 RESULTS AND DISCUSSION

103 **Identification of the genes encoding the NAD⁺-reducing [NiFe]-hydrogenase of *H.*** 104 ***thermoluteolus*.**

105 The draft sequence (published elsewhere) of the *H. thermoluteolus* TH-1^T genome revealed
106 the *HtSH*-related genes, *hoxF*, *hoxU*, *hoxY*, *hoxH*, and *hoxW*, which are apparently arranged
107 as an operon (Fig. 1). Pairwise alignments of *HtSH* and *ReSH* proteins (Fig. S1) revealed
108 40 %, 37 %, 44 %, 46 %, and 26 % identical residues for HoxF, HoxU, HoxY, HoxH, and
109 HoxW, respectively. Notably, the *H. thermoluteolus* TH-1^T genome does not contain a copy
110 of the gene encoding the HoxI protein, which is a constituent of the *ReSH* [24].



111

112 **Fig. 1.** Arrangement of the *HtSH*-related genes (a), proposed subunit/cofactor composition (b), and
 113 observed active site redox states of *HtSH* (c). Genes *hoxF*, *U*, *Y*, and *H* encode the subunits of the
 114 SH protein, while *hoxA* has presumably a regulatory function. Upon insertion of the [NiFe] active site,
 115 the *hoxW* gene product mediates cleavage of a C-terminal extension of the HoxH subunit. The
 116 proposed cofactor composition in b is derived from amino acid sequence comparisons with the
 117 corresponding subunits of *ReSH* and Complex I from *Thermus thermophilus* (see Fig. S1) and
 118 analogies to the well-characterized *ReSH*. The assignment of active site species and their
 119 interconversions shown in c is based on IR and EPR spectroscopic analyses (see below). Redox
 120 states highlighted in green belong to the catalytic conversion of H_2 , while the orange ones represent
 121 inactive states that – except for $\text{Ni}_r\text{-S}$ – require reductive treatment to be converted into the $\text{Ni}_a\text{-S}$
 122 state. The unassigned oxidized state labelled with n/a is unprecedented (see below).
 123

124 Heterologous overproduction and purification of functional *HtSH*

125 For heterologous overproduction of the *HtSH* in *R. eutropha* and subsequent purification,
 126 the *hoxFUYHW* genes were amplified by PCR and put under the control of the native SH
 127 promoter of *R. eutropha* as described in materials and methods. Furthermore, a sequence
 128 encoding the *Strep*-tag II peptide was attached to the 5' end of the *hoxF* gene. The resulting

129 synthetic *hox_{strep}FUYHW* operon was inserted into the broad-host range vector pEDY309
130 resulting in plasmid pJP09, encoding *Strep*-tagged *HtSH*.

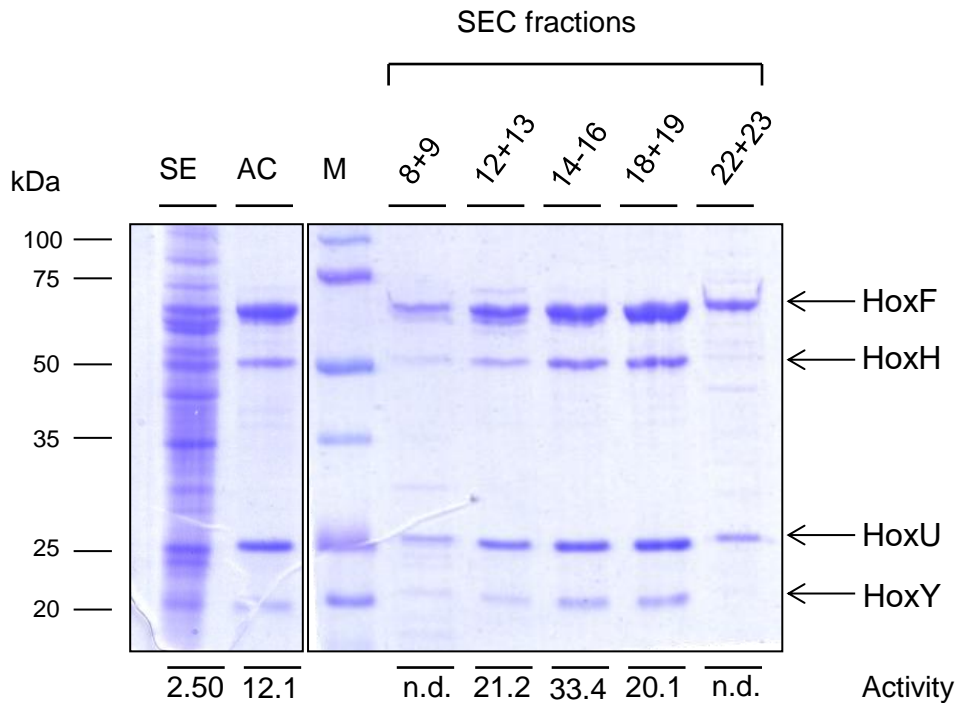
131 For enzyme purification, plasmid pJP09 was transferred into strain *R. eutropha* HF1054,
132 in which the native *hoxFUYHWHI* genes as well as *hoxG* encoding the large subunit of the
133 membrane-bound [NiFe]-hydrogenases have been eliminated by isogenic in-frame deletions.
134 This prevented any “subunit mixing” between *HtSH* and *ReSH* proteins. The transconjugant
135 strain *R. eutropha* HF1054 (pJP09) was cultivated heterotrophically under oxygen-limited
136 conditions as described previously [15,25]. In a first experiment, the H₂-driven NAD⁺
137 reduction activity was measured in soluble extract of the recombinant cells. The activity was
138 2.50 ± 0.12 U mg⁻¹ of protein (Table 1), suggesting the presence of functional *HtSH* proteins.
139 This result also demonstrates that the general [NiFe]-hydrogenase maturation machinery of *R.*
140 *eutropha* [26–28] is able to synthesize and to deliver the active site constituents for the HoxH
141 subunit of *HtSH*.

142 The *HtSH* protein was then purified to homogeneity by *Strep*-Tactin affinity and size
143 exclusion chromatography as described in materials and methods. From 10 g (wet weight) of
144 cells, we routinely obtained 10–12 mg of protein with a specific H₂-driven NAD⁺ reduction
145 activity of 33.4 ± 0.6 U mg⁻¹ of protein (measured at 50 °C, Table 1). The reverse reaction,
146 namely NADH-driven H₂ production, was catalyzed with an activity of 1.0 ± 0.3 U mg⁻¹ of
147 protein. Using dithionite-reduced methyl viologen (MV) as artificial, low-potential electron
148 donor, the H₂ production activity increased to 30 ± 5 U mg⁻¹ of protein. SDS-PAGE
149 performed with the *HtSH* preparation revealed four protein bands assigned to the subunits
150 HoxFUHY (Fig. 2).

151 **Table 1.** Purification of *HtSH* protein enzyme by affinity chromatography.

Fraction ^a	Volume (mL)	Protein concentration (mg/mL)	Total protein (mg)	Specific activity (U mg ⁻¹) ^b	Total activity (U)	Yield (%)	Enrichment factor
SE	40	29.2	1168	2.5 ± 0.1	2920	100	1
AC	1.4	29.7	41.6	12.1 ± 0.1	502	17	4.8
SEC	2.4	4.9	11.7	33.4 ± 0.6	391	13	13.4

152 ^aThe *HtSH* protein was purified from soluble cell extracts (SE) by *Strep*-Tactin affinity chromatography
 153 (AC) and subsequent size exclusion chromatography (SEC) as described in materials and methods.
 154 ^bActivity was determined by H₂-dependent NAD⁺ reduction in 50 mM bis-Tris, pH 6.5, supplemented
 155 with 1 mM NAD⁺, 0.5 mM NiCl₂, 5 mM MgSO₄, 2 μM FMN, and 0.75 mM TCEP at a temperature of
 156 50 °C. One Unit (U) corresponds to the amount of converted substrate (in μmol) in one minute. Values
 157 of a representative purification are shown.

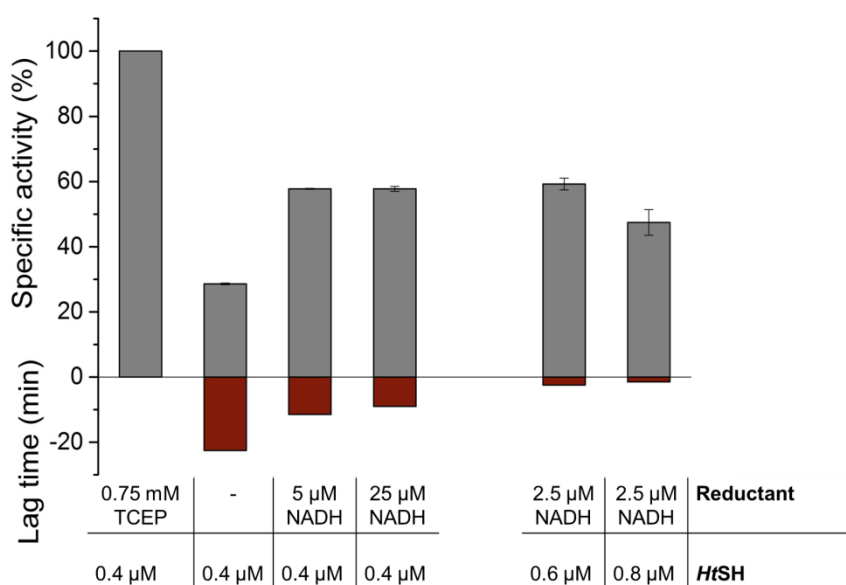


158 **Fig. 2.** Purification of the *HtSH* protein. A protein amount of 30 μg of soluble extract (SE) and 5 μg of
 159 *HtSH* purified by affinity chromatography (AC) and selected fractions (from the subsequent size
 160 exclusion chromatography (SEC) were electrophoretically separated on a 12 % SDS-polyacrylamide
 161 gel and subsequently stained with Coomassie brilliant blue. The specific H₂-driven NAD⁺ reduction
 162 activity (U mg⁻¹ of protein) of each fraction is specified below. Lane M contains marker proteins and
 163 their corresponding molecular weights are given on the left hand side.
 164

165 **Biochemical characterization of purified *HtSH*.**

166 Based on visual inspection of the protein bands after electrophoretic separation (Fig. 2), a
167 ratio of approximately 1:1 of the two SH modules, HoxFU and HoxYH, was obtained only
168 when Ni²⁺ (0.5 mM) and Mg²⁺ (5 mM) ions were present during the whole purification
169 process. A similar observation has been made previously for the NAD⁺-reducing [NiFe]-
170 hydrogenase from *Rhodococcus opacus* [29]. Consequently, the following activity assays
171 were conducted in the presence of Ni²⁺ and Mg²⁺ ions in addition to 2 μM FMN, the latter of
172 which led to a shortened lag phase but did not change the maximal H₂ oxidation activity (Fig.
173 S2). This suggests that FMN serves as an electron acceptor, and reduced FMN can reactivate
174 those inactive *HtSH* species which cannot be activated by H₂ alone. This mechanism is
175 similar to the NADH-based reactivation of as-isolated *ReSH* [24,30]. Highest H₂-driven
176 NAD⁺ reduction activity for purified *HtSH* (Fig. 3), however, was observed when the
177 reductant TCEP (0.75 mM) was added in addition to FMN. Activity was maximal after a lag
178 period of ca. 2.5 min. The removal of just TCEP led to a dramatic increase of the lag time (ca.
179 25 min), and the activity dropped to 25 % of the value measured in the presence of TCEP
180 (Fig. 3). The negative effect of the missing TCEP could be partly compensated through
181 addition of catalytic amounts of NADH (5 μM), which led to the recovery of approx. 50 % of
182 the maximal activity and a halved lag phase (Fig. 3). This indicates that NADH supports
183 reductive reactivation of aerobically purified *HtSH* as previously observed for SH from *R.*
184 *eutropha* [24,30]. A considerable further shortening of the lag phase was accomplished by
185 increasing the protein concentration in the assay. In the presence of 0.8 μM *HtSH* and only
186 2.5 μM NADH, it took only 4 minutes until full activity was developed (Fig. 3). This
187 suggests that the rate of reductive reactivation can also be accelerated by intermolecular
188 electron transfer between individual *HtSH* enzymes. The likelihood of electron exchange
189 between *HtSH* enzymes is of course greater at higher protein concentration.

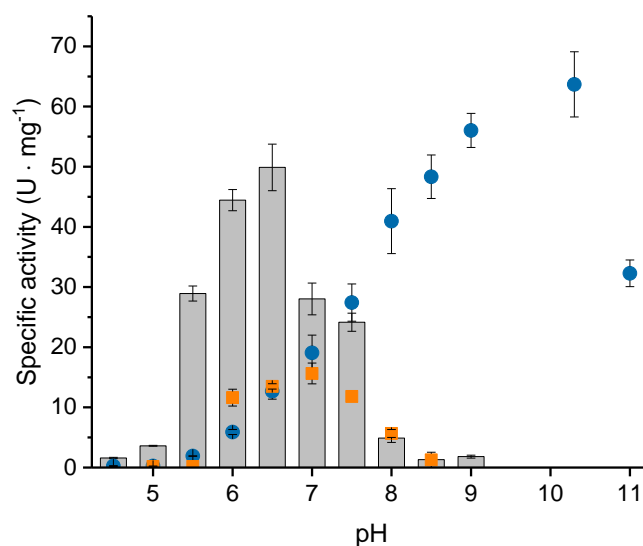
190 Based on the knowledge derived from the experiments described above, NiCl₂, MgSO₄,
 191 FMN, and TCEP were added to the following activity assays, unless stated otherwise. Using
 192 this standard protocol at a fixed temperature of 50 °C, we first determined the H₂-dependent
 193 NAD⁺ reduction activity of purified *HtSH* at different pH values. This was accomplished
 194 with a universal buffer that spanned the entire pH range from pH 4.5–9 (Fig. 4) as well as
 195 with three buffers with different pH ranges (Fig. S3). From both experiments, an optimum pH
 196 of 6.5 was derived. This is in marked contrast to *ReSH* that performs best at pH 8.0 [20,30]
 197 (Table2), where the *H. thermoluteolus* enzyme showed only about 10 % of the maximal H₂-
 198 driven NAD⁺ reduction activity of 50 ± 4 U mg⁻¹ of protein (measured at pH 6.5, Fig. 4).



199
 200 **Fig. 3.** Dependence of H₂-driven NAD⁺ reduction activity of purified *HtSH* protein on the addition of
 201 reductants TCEP and NADH. The assay was performed at 50 °C in 50 mM bis-Tris, pH 6.5,
 202 supplemented with 1 mM NAD⁺, 0.5 mM NiCl₂, 5 mM MgSO₄, 2 μM FMN, and varying amounts of
 203 TCEP, NADH and *HtSH*. The lag time refers to the time elapsed from assay start until full activity was
 204 achieved. 100 % activity refers to 19 U mg⁻¹ of protein.
 205

206 In order to elucidate the origin of the unusual pH optimum, the enzymatic reactions of the
 207 two SH modules were tested separately in a pH-dependent manner (Fig. 4). First, the HoxFU-
 208 catalyzed NADH:benzyl viologen oxidoreductase activity was measured as described in
 209 materials and methods. Maximum activity of 64 ± 5 U ·mg⁻¹ of protein was reached at
 210 approximately pH 10, which is qualitatively consistent with the observations made previously

211 for the HoxFU module of the *ReSH* [31]. The H₂:benzyl viologen oxidoreductase activity of
212 the HoxHY module, however, was found to be optimal at approximately pH 7.0. These
213 results indicate that the pH optimum of the *HtSH* is primarily dictated by the intrinsic bias of
214 the H₂/H⁺-cycling module of the holoenzyme.



215

216 **Fig. 4.** Activity of purified *HtSH* protein at different pH values. The graph depicts the H₂-dependent
217 NAD⁺ reduction activities of *HtSH* (grey bars) as well as the H₂:benzyl viologen (orange symbols) and
218 NADH:benzyl viologen (blue symbols) oxidoreductase activities of the individual *HtSH* modules. The
219 measurements were performed as described in materials and methods with 45 nM of *HtSH* in an
220 universal buffer composed of 16 mM citrate, 16 mM Tris, and 16 mM glycine. Activities were
221 measured at a temperature of 50 °C in the presence of either of 1 mM NAD⁺, 1mM NADH, or 5 mM
222 benzyl viologen, in addition to 0.5 mM NiCl₂, 5 mM MgSO₄, 2 μM FMN, and 0.75 mM TCEP.

223

224

225 **Table 2.** Comparison of soluble, NAD(P)⁺-reducing [NiFe] hydrogenases^a

Organism	<i>H. thermoluteolus</i> TH-1 ^T	<i>R. eutropha</i> H16	<i>Synechocystis</i> sp. PCC 6803	<i>Pyrococcus</i> <i>furius</i>
Designation	SH	SH	bidirectional hydrogenase	SH1
Subunit composition	HoxHYFU	HoxHYFU ₂ [24]	HoxHYFUE [32]	αδβγ [33]
Molecular weight (kDa)	168	207 [24]	180 [32]	153 [33]
K _M H ₂ (μM)	42	37 [30]	11.3 [34] ^b	140 [33]
Physiological electron acceptors/donors	NAD ⁺	NAD ⁺	NAD(P) ⁺ / NAD(P)H, ferredoxin _{red} , flavodoxin _{red} [35,36]	NAD(P) ⁺
K _M NAD(P) ⁺ (μM)	469 (NAD ⁺)	560 (NAD ⁺) [30]	n.p.	40 (NADP ⁺) [33]
k _{cat} for H ₂ -driven NAD(P) ⁺ reduction (s ⁻¹)	150 s ⁻¹	485 s ⁻¹ [8]	n.p.	99 s ⁻¹ (NAD ⁺) [33] 38-89 s ⁻¹ (NADP ⁺) [37]
v _{max} for NAD(P)H-driven H ₂ Production	0.9 U mg ⁻¹	1.2 U mg ⁻¹	2.81 (U mg ⁻¹) [32]	1.5-2 U mg ⁻¹ (NADPH)
T _{opt}	80°C	35°C [20]	60°C [32]	80°C [38,39]
pH _{opt}	6.5	8 [20,30]	6.3 [32]	8.4 [38]
Behavior towards O ₂	moderately O ₂ - tolerant ~50 % H ₂ - dependent NAD ⁺ reduction activity ^c in the presence of 19 μM O ₂	O ₂ -tolerant, ~85% H ₂ - dependent NAD ⁺ reduction activity ^c in the presence of 470 μM O ₂ [15]	O ₂ -sensitive, no catalytic activity in the presence of O ₂ ; can be rapidly reactivated under reducing conditions [40]	moderately O ₂ - tolerant, ~25% of H ₂ oxidation activity ^d in the presence of 14 μM O ₂ [41]

226 ^aNote that values are only limitedly comparable since the assay conditions were not identical.

227 ^bValue has been determined for the bidirectional hydrogenase from the *Synechocystis* sp. relative,
228 *Anabaena variabilis*.

229 ^cCompared to the activity measured in the absence of O₂. Activities were measured
230 spectrophotometrically in solution.

231 ^dCompared to the activity measured in the absence of O₂. Activities were measured electrochemically
232 with immobilized enzyme at oxidizing potential.

233 n.p.; not published

234

235 Measurements of the H₂-dependent NAD⁺ reduction activity of purified *Ht*SH at different

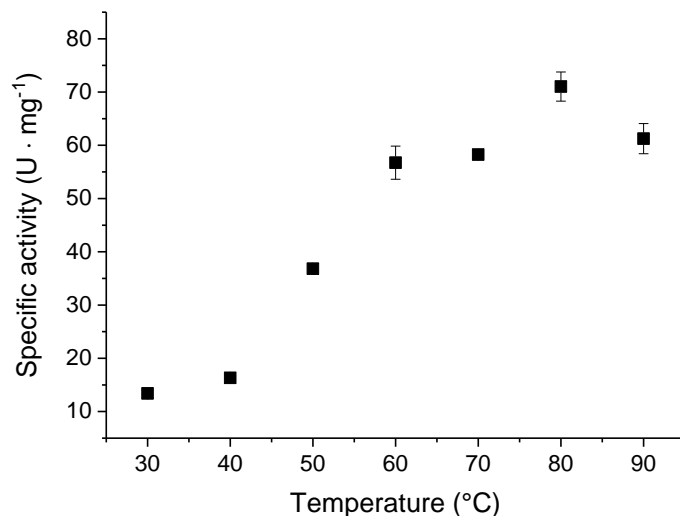
236 temperatures were performed in bis-Tris buffer at pH 6.5 and revealed a maximal activity of

237 71.0 ± 0.3 U mg⁻¹ of protein at a temperature of 80 °C (Fig. 5). This is in sharp contrast to

238 *Re*SH, which quickly loses activity at temperatures higher than 35 °C [20] (Table 2). At

239 33 °C, which is the temperature optimum of *Re*SH activity [30], *Ht*SH showed less than 20 %

240 of the maximal activity.



242

243 **Fig. 5.** Temperature dependence of the H₂-dependent NAD⁺ reduction activity of purified *HtSH*
 244 protein. The measurements were performed as described in materials and methods with 45 nM of
 245 *HtSH* in 50 mM bis-Tris buffer, pH 6.5, containing 1 mM NAD⁺, 0.5 mM NiCl₂, 5 mM MgSO₄, 2 μM
 246 FMN, and 0.75 mM TCEP. If the error bars are not visible, they are equal or smaller than the symbol
 247 size.

248

249 In a next series of experiments, we determined the Michaelis-Menten constants (K_M) for
 250 the natural substrates of the *HtSH*. The K_M value for NAD⁺ was evaluated based on the H₂-
 251 driven NAD⁺ reduction activity of the enzyme and revealed to lie at 469 μM (Fig. S4) which
 252 is close to 560 μM, the value determined for *ReSH* [30]. Activity measurements of the *HtSH*-
 253 mediated benzyl viologen reduction activity in the presence of various NADH concentrations
 254 resulted in a K_M^{NADH} of 1.2 mM (Fig. S5), which is surprisingly high when compared to the
 255 corresponding value of 80 μM determined for the *ReSH* [30]. This suggests that the main
 256 physiological role of *HtSH* enzyme is H₂-driven NAD⁺ reduction.

257 A value of 42 ± 3 μM was determined for the apparent Michaelis-Menten constant, K_M^{app} ,
 258 for H₂ during H₂-driven NAD⁺ reduction of the enzyme (Fig. S6), which is comparable to
 259 that measured for *ReSH* (37 μM, [30], Table 2).

260

261 **Cofactor content and O₂ tolerance of *HtSH***

262 Fluorescence determination revealed 1.07 FMN per SH tetramer. Using inductively
263 coupled plasma optical emission spectrometry, 14.2 ± 0.2 Fe and 2.4 ± 0.1 Ni per SH
264 molecule were detected. On the basis of conserved amino acid residues that are involved in
265 Fe-S cluster coordination in Complex I, 19 iron atoms are expected in addition to one nickel
266 in the catalytic center of the hydrogenase module (Fig. 1, Fig. S1). Additional information on
267 the type of iron-sulfur clusters present in *HtSH* was obtained by nuclear resonance vibrational
268 spectroscopy (NRVS). NRVS is a synchrotron-based vibrational spectroscopic technique that
269 selectively probes iron-specific normal modes and has been shown to provide details on
270 [NiFe]-hydrogenase cofactor structure and composition [42,43]. The partial vibrational
271 density of states (PVDOS) for oxidized *HtSH* is presented in Fig. S7. The band at 414 cm^{-1} is
272 characteristic for the presence of a [2Fe2S] cluster [44], which is supposed to be coordinated
273 by the HoxU subunit. Of the 19 irons in *HtSH*, 16 are expected to be constituents of [4Fe4S]
274 clusters. Indeed, also the spectral pattern between 0 and 400 cm^{-1} is very similar to that of
275 *ReSH* [43] and a [4Fe4S] cluster-containing ferredoxin [45] (Fig. S7), which indicates
276 dominant contributions of [4Fe4S] cluster species. Thus, these results support the presence of
277 four [4Fe4S] clusters and one [2Fe2S] species in *HtSH*.

278 Consistent with the chemolithoautotrophic growth capacity of the host organism under
279 aerobic conditions, the isolated *HtSH* showed sustained H_2 -driven NAD^+ reduction activity in
280 the presence of O_2 (Table 3). However, its O_2 tolerance revealed to be lower than that of the
281 *ReSH* (Table 3, Table 2). While the *ReSH* preserves approximately 100 % activity observed
282 at 20 % O_2 (measured at 30°C in Tris/HCl buffer, pH 8) [14,15], the *H. thermoluteolus*
283 enzyme showed at 10 % O_2 less than 20 % of the activity measured in the absence of O_2 . At 2
284 % O_2 , it displayed only 50 % of the activity observed under anaerobic conditions. However,
285 at low O_2 pressure (0.2 %), *HtSH* activity remained at almost 100 % (Table 3). In this
286 respect, it is noteworthy that the intracellular O_2 concentration in living cells is generally

287 much lower than the external one. This explains why *H. thermoluteolus* cells grow well with
 288 H₂ and CO₂ even at ambient O₂ concentrations, although the isolated enzyme is more O₂
 289 sensitive than the SH from *R. eutropha*.

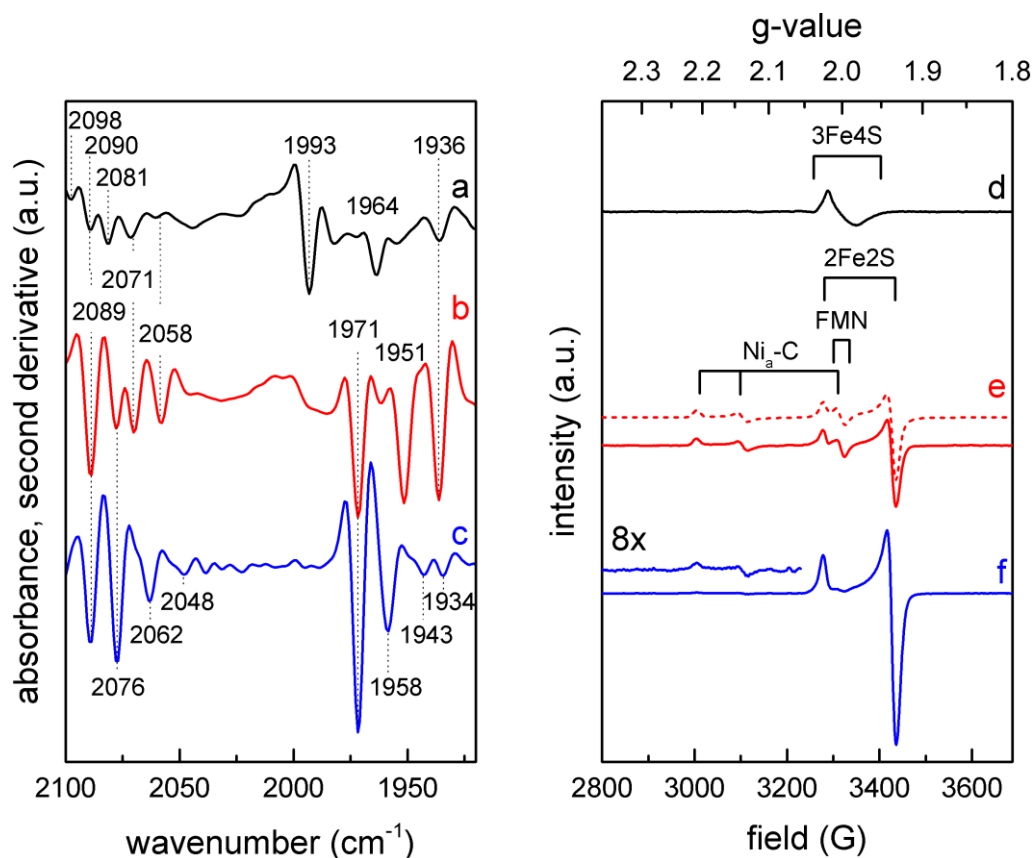
290 **Table 3.** H₂-driven NAD⁺ reduction activity of the *Ht*SH protein^a in the presence of various O₂
 291 concentrations.

O ₂ / H ₂ / N ₂ fractions ^b (% v/v)	[O ₂] (μM)	Hydrogenase activity in the presence of O ₂ (U mg ⁻¹ of protein) ^c	<i>k</i> _{cat} (s ⁻¹)	Hydrogenase activity (%)
0 / 33.33 / 66.66	0.00	16 ± 2	45.9	100
0.2 / 33.33 / 66.46	1,9	15 ± 4	43.0	94.2
2 / 33.33 / 64.66	18,8	7.7 ± 0.3	21.5	49.8
10 / 33.33 / 56.66	94,0	1.3 ± 0.5	3.6	16.6

292 ^a*Ht*SH was purified by affinity chromatography as described in materials and methods. ^bFor each O₂
 293 concentration, a fixed volume of H₂-saturated buffer was mixed with various proportions of O₂- and
 294 N₂-saturated buffers. The gas phase contained the corresponding gas mixtures. ^cH₂-mediated NAD⁺
 295 reduction activity was measured at 50 °C and pH 6.5.

297 Spectroscopic characterization of *Ht*SH

298 To gain insight into structure and function of the metal cofactors, in particular of the [NiFe]
 299 active site, *Ht*SH samples treated with different redox agents were characterized by IR and
 300 EPR spectroscopy. For both types of spectroscopic measurements, samples were prepared
 301 under identical conditions to guarantee comparability of the results. In addition, IR spectro-
 302 electrochemical experiments were performed to provide insight into equilibria between the
 303 individual redox states of the [NiFe] active site. All IR data are displayed as second
 304 derivative spectra where the maximum of an absorption band appears as a sharp negative
 305 peak. Peak positions derived from IR and EPR spectroscopy as well as their assignment to
 306 individual cofactors and redox states are summarized in Table 4 and Table 5, respectively.



307

308 **Fig. 6.** IR (left) and EPR (right) spectra of *HtSH* recorded under different redox conditions. Samples
 309 were prepared as described in materials and methods and measured in the as-isolated, oxidized state
 310 (black spectra) or in their reduced states (red spectra: samples reduced with TCEP and NADH; blue
 311 spectra: samples reduced with TCEP, NADH, and H₂). IR spectra were acquired at 10 °C, while EPR
 312 spectra were recorded at either 10 K (d) or 35 K (e, f).
 313

314 **Table 4.** CO and CN stretching frequencies (cm⁻¹) of IR-spectroscopically observed *HtSH* [NiFe]
 315 active site species.

Assignment	$\nu(\text{CO})$	$\nu(\text{CN})$	
n/a ^a	1993	2081	2090
Ni _r -B-like	1964	2087	2098
Ni _r -S	1936	2058	2071
Ni _a -S	1951	2076	2089
Ni _a -C	1971	2076	2089
Ni _a -SR	1958	2062	2076
Ni _a -SR'	1943	2048	2062
Ni _a -SR''	1934	2048	2062

^aNot assigned. Oxidized active site species of unknown structure

316

317

318 **Table 5.** g-values of *HtSH* cofactor species observed by EPR spectroscopy.

Assignment	g ₁	g ₂	g ₃
[3Fe4S]	2.004	1.982	
[2Fe2S]	2.026	1.935	
[NiFe]: Ni _a -C	2.210	2.139	2.013
[NiFe]: n/a ^a	2.260	2.127	2.034
FMN	2.003		

^aNot assigned.

319

320 IR spectra of as-isolated *HtSH* exhibit up to three distinct bands at 1993, 1964, and
 321 1936 cm⁻¹ (Fig. 6, trace a). Signals in this spectral region are generally associated with the
 322 stretching vibration of the intrinsic CO ligand of the [NiFe] active site, and different
 323 vibrational frequencies reflect distinct redox/structural states of this cofactor [3,46–49]. The
 324 three individual CO stretching vibrations of oxidized *HtSH* are separated by approximately
 325 30 cm⁻¹, which is exceptional for active site species of oxidized [NiFe] hydrogenases. This
 326 observation suggests that the active site of as-isolated *HtSH* can adopt three configurations
 327 that strongly differ in terms of structural and/or electronic properties. The signal at 1964 cm⁻¹
 328 may reflect the apparently EPR-silent “Ni_r-B-like” state (Fig. 1), which was previously
 329 detected for *ReSH* and other NAD(P)⁺-reducing [NiFe] hydrogenases [6,8,12,40,50,51], and
 330 the band at 1936 cm⁻¹ is assigned to the Ni_r-S state (see below). The signal at 1993 cm⁻¹,
 331 however, is unprecedented and absent in as-isolated *ReSH* [8,50,52–54]. According to
 332 relative intensities of the CO stretching bands, the contributions of the three different states
 333 varied across different as-isolated *HtSH* preparations. The unusual signal at 1993 cm⁻¹,
 334 however, generally represented the dominant species. To the best of our knowledge, such a
 335 high CO stretching frequency has not been observed for any [NiFe] hydrogenase to date. This
 336 suggests unusually high oxidation states of the metal ions, e.g. formation of ferric iron [55],
 337 or unusual structural features at or in close vicinity of the [NiFe] active site. In general, such
 338 observations and the appearance of multiple oxidized states may result from the contact with

339 O₂ during and after protein isolation [50,56]. Importantly, all IR-spectroscopically detected
340 oxidized species of the *HtSH* active site can be activated under reducing conditions (Fig. 6,
341 traces b and c), as observed previously for, e.g., *ReSH* [50]. This indicates that the
342 modifications reflected by the unusual signal at 1993 cm⁻¹ are reversible and not related to
343 oxidative damage.

344 The EPR spectrum of as-isolated *HtSH* was measured at 10 K (Fig. 6, trace d) and
345 exhibits a minor signal, presumably related to a [3Fe4S] cluster. Since no such cofactor is
346 expected for native *HtSH*, this feature likely reflects the (partial) oxidative damage of one or
347 more [4Fe4S] clusters, which is in line with preparation-dependent variations of the signal
348 intensity. This situation is reminiscent of *ReSH* and the related NAD⁺-reducing hydrogenase
349 from *Rhodococcus opacus* (*Ro*), both of which exhibit similar signals related to (non-native)
350 [3Fe4S] species [8,13,53,57–60]. Furthermore, a weak rhombic signal, detected at 35 K, (Fig.
351 S8, trace a) is presumably related to a paramagnetic [NiFe] active site state of as-isolated
352 *HtSH*. Signals related to typical active site species of oxidized “standard” [NiFe]
353 hydrogenases, however, were not detected, which is consistent with previous findings for
354 NAD(P)⁺-reducing hydrogenases from other organisms. [6,8,12,13,40,53,57–61]

355 Upon addition of the mild reducing agents TCEP and NADH to as-isolated *HtSH*,
356 bands at 1993 and 1964 cm⁻¹ disappeared from the IR spectrum in favor of two new
357 absorption features at 1971 and 1951 cm⁻¹ (Fig. 6, trace b). The former is ascribed to the
358 Ni_a-C state of the enzyme, which is in line with previous studies showing that Ni_a-C exhibits
359 the highest CO stretching frequency among all catalytically active [NiFe] species [3]. The
360 second band, observed at 1951 cm⁻¹, is assigned to the one-electron more oxidized Ni_a-S
361 state, consistent with an intensity decrease upon hydrogen incubation of the enzyme (see
362 below and Fig. 6, trace c). In *ReSH* and soluble hydrogenase I (SH1) from the
363 hyperthermophilic organism *Pyrococcus furiosus* (*Pf*), this state corresponds to signals at

364 1946 cm^{-1} [50] and 1950 cm^{-1} [51], respectively (note that *PfSH1* differs from *HtSH* and
365 *ReSH* in terms of its subunit and cofactor composition [6]). The band at 1936 cm^{-1} gains
366 intensity upon incubation of as-isolated *HtSH* with TCEP and NADH (Fig. 6, traces a and b)
367 indicating that it reflects a partially reduced [NiFe] species with a formal Ni^{II} oxidation state.
368 Since this CO stretching frequency is clearly lower than those observed for most other *HtSH*
369 [NiFe] active site species, we tentatively assign this intermediate to the deprotonated $\text{Ni}_r\text{-S}$
370 subspecies, which features a bridging OH^- ligand.

371 The corresponding EPR spectrum of TCEP/NADH-reduced *HtSH* was recorded at
372 35 K and clearly shows the hydride-containing $\text{Ni}_a\text{-C}$ state (Ni^{III} , $S = 1/2$), consistent with the
373 corresponding assignment of the strong IR absorbance at 1971 cm^{-1} . Moreover, signals
374 attributed to a [2Fe2S] cluster (constituent with the results obtained by NRVs, Fig. S7) and a
375 flavin radical species were detected (Fig. 6, trace e). These assignments are supported by
376 simulation and subsequent summation of the individual components (Fig. 6, trace e, dashed
377 line) and consonant with previous assignments for *ReSH* and *RoSH* [8,12,13,40,53,57–
378 60,62]. Measurements performed at 10 K (Fig. S8, trace b) revealed an additional broad
379 signal at $g = 1.85$, possibly reflecting a [4Fe4S] cluster.

380 Upon incubation of *HtSH* with H_2 (in the presence of TCEP and NADH), the 1971
381 cm^{-1} band, assigned to the $\text{Ni}_a\text{-C}$ state, becomes the most intense signal of the IR spectrum,
382 and corresponding CN stretching vibrations of this catalytic intermediate can be identified at
383 2076 and 2089 cm^{-1} (Fig. 6, trace c). Moreover, a new redox species is formed as indicated
384 by the appearance of an absorption band at 1958 cm^{-1} (Fig. 6, trace c). According to spectro-
385 electrochemical measurements (Fig. S9, traces b and c), an enrichment of this species
386 requires lower potentials than that of the $\text{Ni}_a\text{-C}$ state. Therefore, we attribute this signal to the
387 fully reduced $\text{Ni}_a\text{-SR}$ species with corresponding CN stretching bands at 2076 and 2062 cm^{-1} ,
388 which is in line with band assignments for *PfSH1* [51]. In case of *ReSH*, a similar set of

389 signals, including an identical CO stretching band at 1958 cm^{-1} , has been assigned to the
390 $\text{Ni}_a\text{-SR2}$ state [6,12,50]. In the current case, however, this assignment is less plausible since
391 CO stretching bands of *HtSH* active site redox states appear to be generally higher in
392 frequency than their counterparts in *ReSH*. Two further weak bands at 1943 and 1934 cm^{-1}
393 (Fig. 6, trace c) might reflect $\text{Ni}_a\text{-SR}'$ and $\text{Ni}_a\text{-SR}''$ subspecies of the reduced state [12,50].
394 Consistently, these states were observed as bands at 1940 ($\text{Ni}_a\text{-SR}'$) and 1931 cm^{-1} ($\text{Ni}_a\text{-SR}''$)
395 for *PfSH1*, which also exhibits generally higher CO stretching frequencies than *ReSH* [51].
396 Observation of these two subspecies provides further support for the assignment of the 1958
397 cm^{-1} band to $\text{Ni}_a\text{-SR}$ as there is no other signal in the IR spectrum of *HtSH* that could be
398 attributed to the main component of this species.

399 The EPR spectrum of H_2 -incubated *HtSH*, recorded at 35 K , is dominated by the
400 signal of the $[\text{2Fe2S}]$ cluster (Fig. 6, trace f) confirming further enzyme reduction. In contrast
401 to the IR data, this EPR spectrum exhibits only trace amounts of the $\text{Ni}_a\text{-C}$ state. However, in
402 addition to broad features at positions typical for reduced $[\text{4Fe4S}]$ cofactors ($g = 1.83$), an
403 EPR spectrum recorded at 6.5 K (see Fig. S8, trace c) reveals pronounced broadened signals
404 in the field range characteristic for the $\text{Ni}_a\text{-C}$ state, indicating strong magnetic coupling of the
405 active site with another paramagnetic species. This temperature dependence of the $\text{Ni}_a\text{-C}$
406 signal pattern can be explained by fast spin-lattice relaxation of an Fe-S cluster near the
407 $[\text{NiFe}]$ site, leading to enhanced relaxation and broadening of the $\text{Ni}_a\text{-C}$ signal until its
408 disappearance at higher temperatures. Similar magnetic interactions have been described in
409 detail for “standard” $[\text{NiFe}]$ hydrogenases [63,64], and particularly pronounced coupling
410 effects were also reported for *PfSH1* [39], *Pyrococcus furiosus* ferredoxin [65], and
411 individual clusters of homologous respiratory Complex I [66–68]. For the $\text{Ni}_a\text{-C}$ state of
412 *HtSH*, this effect appears to be most pronounced for the NADH/TCEP/H_2 -treated sample.
413 Assuming that unspecific, preparation-dependent effects can be excluded, this observation

414 suggests that spin-lattice relaxation is accelerated by coupling to a paramagnetic cofactor
415 ([4Fe4S] species) that is barely reduced by TCEP/NADH alone.

416 To support band assignments and gain insight into the reversibility of redox reactions
417 at the [NiFe] active site of *HtSH*, initial IR spectro-electrochemical measurements and gas-
418 exchange experiments were performed (Fig. S9, Fig. S10). As summarized in Table 4, these
419 studies allowed a preliminary assignment of the CN stretching bands for all detected [NiFe]
420 active site states. The monitored interconversions also confirmed the above-made
421 assignments of the individual [NiFe] active site species, and the corresponding redox
422 equilibria could be established (Fig. 1c). Remarkably, after reduction of as-isolated *HtSH* and
423 subsequent re-oxidation, the [NiFe] active site species reflected by the unusual 1993 cm^{-1}
424 band did not re-appear (Fig. S9, Fig. S10). Thus, we propose that the reaction resulting in this
425 particular species is kinetically hindered, suggesting a pronounced structural reorganization.
426 In line with the unusually high CO stretching frequency, this observation supports the idea
427 that this oxidized state differs considerably from other typical [NiFe] active site
428 intermediates.

429

430 CONCLUSION

431 Here, we provide the first combined biochemical and spectroscopic characterization of a
432 NAD^+ -reducing [NiFe]-hydrogenase that is both thermostable and O_2 -tolerant. The enzyme
433 originates from the thermophile *Hydrogenophilus thermoluteolus* TH-1^T [21], and its
434 corresponding structural genes were heterologously overexpressed in the mesophilic host
435 *Ralstonia eutropha* H16. This procedure resulted in the formation of catalytically active
436 *HtSH* protein, which clearly shows that the hydrogenase-specific maturation machinery from
437 *R. eutropha* [5] is capable of synthesizing and inserting the $\text{NiFe}(\text{CN})_2\text{CO}$ cofactor into the
438 large hydrogenase subunit of *HtSH*. Taking into account the successful heterologous

439 overproduction of SH from *Rhodococcus opacus* [69], *R. eutropha* seems to be an excellent
440 host for synthesis and isolation of catalytically active SH proteins from bacterial species that
441 are so far unamenable to genetic engineering.

442 Table 2 shows biochemical and structural properties of the *HtSH* in comparison with those of
443 other soluble NAD(P)⁺-reducing [NiFe]-hydrogenases. The isolated *HtSH* is a
444 heterotetrameric enzyme with a turnover frequency of ca. 150 s⁻¹ for H₂-driven reduction of
445 NAD⁺ at pH 6.5 and 50 °C. In terms of biotechnologically relevant cofactor regeneration [19],
446 the *HtSH* is complementary to *PfSH1*, which preferably reduces NADP⁺ in a H₂-dependent
447 manner at high temperature [33]. Although to a lesser extent when compared to *ReSH*, *HtSH*
448 shows catalytic H₂-mediated NAD⁺ reduction in the presence of O₂ in solution assays. For
449 *PfSH1*, O₂-tolerant H₂ oxidation (but not NAD(P)⁺ reduction) has so far only been shown
450 electrochemically with immobilized enzyme [41]. Though phylogenetically closely related to
451 *HtSH* and *ReSH*, the purified bidirectional [NiFe]-hydrogenase from *Synechocystis* sp. seems
452 to be rather unstable and is rapidly inactivated by O₂. The well-characterized and
453 extraordinary O₂-tolerant *ReSH*, in contrast, shows good stability and highest activity at
454 moderate temperatures and pH 8, but quickly loses activity at temperatures above 35 °C [20].
455 In summary, the *HtSH* represents an attractive candidate for biotechnological applications,
456 e.g., as an NADH regeneration catalyst in enzymatic cascades that rely on high temperatures
457 and O₂ as a co-substrate.

458 EPR, IR and NRV spectroscopic analyses of the *HtSH* protein revealed the occurrence of
459 FMN, [2Fe2S], and [4Fe4S] cluster species as well as typical active site states that have been
460 observed for other soluble NAD(P)⁺-reducing [NiFe] hydrogenases [6,40,51]. These include
461 the Ni_I-B-like state that is not directly involved in H₂/H₊ cycling as well as the Ni_a-S, Ni_a-C,
462 and Ni_a-SR states which are generally accepted to be intermediates of the catalytic cycle.
463 While the Ni_a-C state was identified both by IR and EPR spectroscopy, all other states are

464 EPR-silent and were assigned based on IR spectroscopic analyses only. Interestingly, the
465 Ni_a-C signal in the EPR spectrum of H₂-treated *HtSH* was mainly observed at temperatures
466 below 10 K, presumably due to fast spin-lattice relaxation related to magnetic coupling with
467 another cofactor that is paramagnetic under these reducing conditions. This observation
468 represents an important finding that could explain why Ni_a-C and other paramagnetic active
469 site species have often not been observed for NAD(P)⁺-reducing [NiFe] hydrogenases [6,40].
470 Furthermore, the as-isolated, oxidized *HtSH* exhibits a CO stretching vibration at 1993 cm⁻¹,
471 which is extremely high in frequency and so far unprecedented for [NiFe]-hydrogenases. This
472 unusual vibrational band most likely reflects an alternative geometry and/or coordination
473 environment of the hetero bimetallic active site. Since no crystallographic data is available
474 yet, further spectroscopic investigations are currently in progress to gain detailed insight into
475 the structure this novel species.

476

477 **Materials and methods**

478 **Construction of the synthetic P_{SH}-*hox*_{strep}*FUYHW* operon, growth conditions, and**
479 **protein purification.**

480 The *Ht*SH-derived gene cluster containing *hoxFUYHW* was amplified by PCR using the
481 primers

482 5'-agaacctgtacttccagggcgcaacacgaggaggaggaac-3'

483 and

484 5'-ctcggtagccgggatccatacctctctctctggtgaaaaaac-3',

485 and genomic DNA from *Hydrogenophilus thermoluteolus* TH-1^T as the template. The
486 underlined bases of the primers are complementary to plasmid pGE837, which is a pCM66
487 [70] derivative carrying a XbaI-BamHI-cut fragment from plasmid pGE770 [15] with P_{SH}-
488 *Strep**hoxF* from *Ralstonia eutropha* H16 followed by a sequence encoding a GGGENLYFQG
489 linker with a TEV cleavage site (underlined residues). Plasmid pGE837 was linearized by
490 inverted PCR using primers 5'-atggatccccgggtaccga-3' and 5'-gccctggaagtacaggttctcg-3', and
491 the 7.9-kb product served as recipient of the *Ht hoxFUYHW* PCR amplicon, which was
492 inserted according to the Gibson Assembly® manual (New England BioLabs). The resulting
493 plasmid carries the *Ht hoxFUYHW* genes under control of the SH promoter of *R. eutropha*
494 [71], whereby the 5' end of the *hoxF* gene was equipped with a linker sequence and a *Strep*-
495 tag II-encoding sequence. A P_{SH}-*hox*_{strep}*FUHYW* fragment was cut out with Eco53KI and
496 XbaI, and the resulting 5.7 kb fragment was inserted into the ScaI-XbaI-cut vector pEDY309
497 [72]. This yielded plasmid pJP09, which was subsequently transferred by conjugation to *R.*
498 *eutropha* HF1054, which is a HF424 [73] derivative carrying an additional in-frame deletion
499 in the *hoxI* gene.

500 Strain *R. eutropha* HF1054 (pJP09) was grown heterotrophically in a mineral salts medium
501 containing a mixture of 0.05 % (w/v) fructose and 0.4 % (v/v) glycerol (FGN medium) at

502 30 °C as described previously [25]. Upon reaching an optical density at 436 nm of 9–11, the
503 culture was collected, and the cells were harvested by centrifugation at $8850 \times g$ for 15 min at
504 4 °C. The cell pellet was resuspended in 50 mM KPO_4 , pH 7.2, containing 15–20 % (v/v)
505 glycerol, 5mM $MgCl_2$, 0.5 mM $NiCl_2$, and protease-inhibitor cocktail (EDTA-free Protease
506 Inhibitor, Roche). The extract was furthermore supplemented with 5 mM NAD^+ in order to
507 keep the *HtSH* in the oxidized state, which is thought to prevent extensive oxidative damage
508 through reactive oxygen species [15]. After two passages through a chilled French press cell
509 at a pressure of 125 MPa, the soluble extract was separated from solid cell constituents by
510 centrifugation at $72500 \times g$ for 45 min. The supernatant was loaded onto a 2 mL *Strep*-Tactin
511 Superflow column (IBA), which was previously equilibrated with resuspension buffer. After
512 washing with at least 6 column volumes of resuspension buffer, the protein was eluted in
513 resuspension buffer containing 5 mM desthiobiotin. A final concentration of 20–30 mg ml⁻¹
514 of purified protein was achieved after concentration with Ultra Centrifugal Filter Units
515 (Amicon).

516 In order to obtain *HtSH* protein with homogenous subunit stoichiometry, size exclusion
517 chromatography was conducted after affinity chromatography. An amount of 200 µL of the
518 concentrated *HtSH* eluate was loaded onto a Superdex 200 10/300 GL column which was
519 previously equilibrated with the same buffer used for affinity chromatography. Using an
520 ÄKTA pure system, the flow rate was held at 0.2 mL min⁻¹, and protein elution occurred at
521 approximately 0.3 column volumes as observed by an UV/vis absorption increase at 280 nm
522 and 420 nm. Protein fractions of 0.4 mL were collected, and the *HtSH* subunit composition
523 was checked by SDS-PAGE according to Laemmli et al. [74]. After determining the H₂-
524 dependent reduction of NAD^+ activity, fractions with highest specific activities and
525 homogeneity were pooled and again concentrated using Ultra Centrifugal Filter Units
526 (molecular weight cut-off of 100 kDa).

527 **Enzyme assays.** All enzyme measurements were performed in the presence of defined gas
528 mixtures unless stated otherwise. Prior to use in enzyme assays, the buffers were bubbled
529 with the respective gases. Buffers with 100 % gas-saturation (1 bar, 50 °C) contained 720 μM
530 H₂, 940 μM O₂ or 483 μM N₂. Buffers containing gas mixtures were prepared by mixing
531 individual buffers with 100 % gas saturation. The head space of the reaction vessels was kept
532 as small as possible to avoid degassing of solutions. H₂-driven NAD⁺ reduction of purified
533 *HtSH* in soluble extracts was determined at 50 °C in a buffer-filled, rubber-stoppered cuvette.
534 The reactions were started by the addition of enzyme, and the absorbance increase at 365 nm
535 due to NADH accumulation was monitored spectrophotometrically with a Cary 50 (Varian).
536 The pH-dependent *HtSH* activity was measured by using two different strategies. First, to
537 minimize the influence of different buffer components on SH activity, a broad-range buffer
538 system (pH 4.5–9) composed of 16 mM citrate, 16 mM Tris, and 16 mM glycine was used.
539 The buffer system was adjusted at 50 °C with appropriate acids or bases to the desired pH
540 values. Second, SH activity was also tested in the individual buffers mentioned above.
541 Temperature-dependent activity measurements were performed in 50 mM bis-Tris, pH 6.5,
542 containing 0.75 mM TCEP (replacing DTT), 0.5 mM NiCl₂, 5 mM MgCl₂ and 2 μM FMN.
543 This owes to the fact that DTT precipitates in NiCl₂- and MgCl₂-containing 50 mM KPO₄
544 buffer at temperatures above 40 °C.
545 NADH-driven H₂ production was measured with a modified Clark-type electrode [75] at
546 50 °C in 50 mM bis-Tris, pH 6.5, containing 5 mM MgCl₂, 0.5 mM NiCl₂, 0.75 mM TCEP, 2
547 μM FMN and 1 mM NADH. The buffers as well as the additives were gassed with N₂ before
548 mixing, and the reaction was started by the addition of enzyme. Diaphorase activity of the SH
549 was recorded spectrophotometrically as NADH-dependent benzyl viologen reduction at
550 50 °C in buffers with different pH values (composition see above), containing 5 mM benzyl
551 viologen (BV), 1 mM NADH, and 90 μM dithionite. H₂-dependent reduction of BV (5 mM)

552 was tested at 50 °C in buffers with different pH values (composition see above). Prior to use,
553 the buffers were saturated with H₂.

554 In order to determine affinity constants for NAD⁺ or NADH, the initial reaction velocities for
555 H₂-dependent NAD⁺ and NADH-dependent BV reduction, respectively, were measured at
556 50 °C and varying substrate concentrations. The recorded slopes were plotted against the
557 substrate concentration and fitted to the Michaelis-Menten kinetic using the program Origin
558 2016.

559 Determination of affinity towards H₂ was performed amperometrically by mixing different
560 volumes of H₂- and N₂-saturated buffers (50 mM bis-Tris, pH 6.5, 5 mM MgCl₂, 0.5 mM
561 NiCl₂) to a total volume of 1.3 mL in the reaction chamber of a modified Clark electrode. The
562 assay contained further the natural electron acceptor, NAD⁺ (1 mM), in addition to 0.75 mM
563 TCEP, and 2 μM FMN. The reaction was started by enzyme addition, and the resulting
564 current change was recorded. The derived reaction velocities were plotted against the H₂
565 concentration and fitted to the Hill equation using Origin 2016.

566 **Protein, iron, and FMN determination.** The protein concentration was determined with the
567 BCATM Protein Assay Reagent Kit (Pierce, USA) using bovine serum albumin as the
568 standard. The flavin mononucleotide concentration in protein samples was analyzed
569 fluorometrically as described previously [30,31] Iron and nickel contents of purified *HtSH*
570 samples were analyzed by inductively coupled plasma optical emission spectroscopy (ICP-
571 OES) as previously described [76]. Final numbers were derived from two biological
572 replicates, while each sample was measured three times (three technical replicates).

573 **Sample preparation for IR and EPR spectroscopy.** For the characterization of as-isolated
574 *HtSH*, protein fractions were concentrated to approx. 0.3 mM using Amicon Ultra 0.5 mL
575 Centrifugal Filters (Merck KGaA) and measured without further treatment. Samples of
576 reduced *HtSH* were prepared using different procedures. Prior to all reductive treatments,

577 buffers were purged with Ar for 30 min, and O₂ was removed from protein samples by ten
578 consecutive cycles of Ar purging and vacuum exertion. Partial reduction of the enzyme was
579 achieved by 30 min incubation of 0.03 mM *Ht*SH with 2 mM TCEP and 5 mM NADH at
580 50 °C in an anaerobic, N₂-filled glovebox. After these treatments, the samples were
581 concentrated to approx. 0.3 mM, and IR transmission cells and EPR tubes were purged with
582 N₂ prior to loading. To further reduce *Ht*SH, solutions containing 0.03 mM of protein were
583 incubated with 2 mM TCEP, 5 mM NADH, and 1 bar O₂-free H₂ (O₂ was removed using a
584 Varian Gas Clean Oxygen Filter PIN CP17970) in H₂-saturated buffer at 50 °C for 30 min in
585 an anaerobic chamber (95 % N₂, 5 % H₂). The H₂ stream was enriched with H₂O to avoid
586 sample drying. Prior to measurements, samples were concentrated to ~ 0.3 mM, and IR
587 transmission cells and EPR tubes were purged with H₂. Aliquots of all samples were directly
588 injected into an IR transmission cell for subsequent characterization, while the remainder was
589 transferred to EPR tubes, quenched in cold ethanol (ca. 210 K) and stored in liquid nitrogen
590 for further analysis.

591 **IR spectroscopy.** IR spectra of 0.3 mM solutions of as-isolated and chemically reduced
592 *Ht*SH were recorded with a spectral resolution of 2 cm⁻¹ using a Bruker Tensor 27 FTIR
593 spectrometer, equipped with a liquid nitrogen-cooled MCT detector. The sample
594 compartment was purged with dry air, and the sample was held in a temperature-controlled
595 (10 °C) gas-tight IR transmission cell for liquid samples (volume: 10 μL, optical path length:
596 50 μm), equipped with CaF₂ windows. The Bruker OPUS software, version 5.5 or higher,
597 was used for data acquisition and evaluation.

598 **IR spectro-electrochemical experiments.** IR spectro-electrochemical experiments were
599 performed on ca. 0.3 mM solutions of *Ht*SH, activated anaerobically with 2 mM TCEP, using
600 an Optically Transparent Thin Layer Electrochemical (OTTLE) cell [77] with an optical path
601 length below 10 μm. In order to avoid protein adsorption, the gold mesh working electrode

602 was incubated anaerobically with a mixed self-assembling monolayer of 1 mM cysteamine
603 and 1 mM mercaptopropionic acid, solved in ethanol, for 30 min. Preparation of the OTTLE
604 cell was performed anaerobically in an Ar-filled box. The following redox mediators were
605 added to the protein solution in order to ensure fast equilibration at the applied potentials (0.5
606 mM each, potential vs. SHE): TMPPO (+262 mV), 1,2-naphthoquinone (+145 mV), 1,4-
607 naphthoquinone (+60 mV), methylene blue (+11 mV), indigo trisulfate (-80 mV), indigo
608 disulfate (-130 mV), 2-hydroxy-1,2-naphthoquinone (-139 mV), resorufin (-195 mV),
609 anthraquinone-2-sulfonate (-225 mV), safranin T (-290 mV), benzyl viologen (-358 mV),
610 methyl viologen (-446 mV) [77–79]. Potential-dependent IR spectra with a resolution of 2
611 cm^{-1} were recorded at 30 °C using a Bruker IFS 66 FTIR spectrometer equipped with a liquid
612 nitrogen-cooled MCT detector. The Bruker OPUS software, version 5.5 or higher, was used
613 for data acquisition and evaluation. Potential control was accomplished using a Model 263A
614 Potentiostat (Princeton Applied Science) and the PARControl 1.05 software. Samples were
615 equilibrated at all potentials for at least 3 min until the corresponding IR spectrum remained
616 unchanged.

617 **EPR spectroscopy.** A Bruker EMXplus spectrometer equipped with an ER 4122 SHQE
618 resonators and an Oxford EPR 900 helium flow cryostat with temperature control (Oxford
619 ITC4) between 5 and 310 K was used in the experiments. Spectra were baseline-corrected by
620 subtracting a background spectrum obtained from buffer solution using the same
621 experimental parameters. Experimental conditions: 1 mW microwave power, microwave
622 frequency: 9.29 GHz, 1 mT modulation amplitude, 100 kHz modulation frequency. Spectra
623 simulations were performed using the MATLAB toolbox EasySpin (version 5.1.7).

624 **NRVS spectroscopy.** For nuclear resonance vibrational spectroscopy (NRVS), *R. eutropha*
625 HF1054 (pJP09) was cultured as described above, with the exception that 18 μM $^{57}\text{FeCl}_2$
626 instead of $^{56}\text{FeCl}_2$ was used as the iron source. The resulting ^{57}Fe -labelled *HtSH* was purified

627 via *Strep*-Tactin affinity chromatography. NRVS was performed at SPring-8 BL09XU with a
628 0.8 meV (6.5 cm^{-1}) energy resolution at 14.4125 keV as described previously [43]. The beam
629 size at BL09XU was 1.1 mm (horizontal) \times 0.6 mm (vertical). A 4-element avalanche photo
630 diode detector array was used to measure delayed K shell fluorescence and nuclear
631 fluorescence by ^{57}Fe atoms. All measurements were performed in the cryostat base that was
632 cooled to 10 K. The real sample temperature was 30–60 K, as obtained from the spectral
633 analysis. The raw NRVS data was converted to a ^{57}Fe partial vibrational density of states
634 (PVDOS) by the PHOENIX software [80], while the energy scale was calibrated with an
635 external reference ($[\text{NEt}_4][\text{FeCl}_4]$). For the *HtSH* protein sample (22 μl , 0.8 mM), the
636 accumulation time was 21 h.

637

638 ***Acknowledgements***

639 We are grateful to Thomas Lonsdale (University of Oxford) for initial biochemical analyses
640 of purified *HtSH*. We thank the group of Professor Silke Leimkühler (Universität Postdam)
641 for metal determination. J.P. and S.W. are grateful for receiving scholarships from the Berlin
642 International Graduate School for Natural Science & Engineering (BIG-NSE). This work was
643 supported by the Deutsche Forschungsgemeinschaft (DFG) through the Cluster of Excellence,
644 Unifying Concepts in Catalysis (UniCat, EXC 314), and the priority program “Iron-Sulfur for
645 Life” (SPP 1927). The NRVS experiments were performed at BL09XU of SPring8 approved
646 under JASRI proposal number 2014B1032. S. P. Cramer is indebted to the Einstein
647 Foundation (Berlin) for support through an Einstein Visiting Fellowship.

- 649 [1] P.M. Vignais, B. Billoud, Occurrence, classification, and biological function of
650 hydrogenases: an overview, *Chem. Rev.* 107 (2007) 4206–4272.
- 651 [2] E. Schwartz, J. Fritsch, B. Friedrich, H₂-Metabolizing Prokaryotes, in: E. Rosenberg, E.F.
652 DeLong, S. Lory, E. Stackebrandt, F. Thompson (Eds.), *The Prokaryotes*, Springer Berlin
653 Heidelberg, Berlin, Heidelberg, 2013, pp. 119–199.
- 654 [3] W. Lubitz, H. Ogata, O. Rüdiger, E. Reijerse, Hydrogenases, *Chem. Rev.* 114 (2014)
655 4081–4148.
- 656 [4] J. Fritsch, O. Lenz, B. Friedrich, Structure, function and biosynthesis of O₂-tolerant
657 hydrogenases, *Nat. Rev. Microbiol.* 11 (2013) 106–114.
- 658 [5] O. Lenz, L. Lauterbach, S. Frielingsdorf, B. Friedrich, Oxygen-tolerant hydrogenases and
659 their biotechnological potential, in: M. Rögner (Ed.), *Biohydrogen*, De Gruyter, 2015, pp.
660 61–88.
- 661 [6] M. Horch, L. Lauterbach, O. Lenz, P. Hildebrandt, I. Zebger, NAD(H)-coupled hydrogen
662 cycling - structure-function relationships of bidirectional [NiFe] hydrogenases, *FEBS Lett.*
663 586 (2012) 545–556.
- 664 [7] E. van der Linden, B.W. Faber, B. Bleijlevens, T. Burgdorf, M. Bernhard, B. Friedrich,
665 S.P. Albracht, Selective release and function of one of the two FMN groups in the
666 cytoplasmic NAD⁺-reducing [NiFe]-hydrogenase from *Ralstonia eutropha*, *Eur. J.*
667 *Biochem.* 271 (2004) 801–808.
- 668 [8] E. van der Linden, T. Burgdorf, A.L. de Lacey, T. Buhrke, M. Scholte, V.M. Fernandez,
669 B. Friedrich, S.P. Albracht, An improved purification procedure for the soluble [NiFe]-
670 hydrogenase of *Ralstonia eutropha*: new insights into its (in)stability and spectroscopic
671 properties, *J. Biol. Inorg. Chem.* 11 (2006) 247–260.
- 672 [9] R.G. Efremov, L.A. Sazanov, The coupling mechanism of respiratory complex I - A
673 structural and evolutionary perspective, *Biochim. Biophys. Acta.* 1817 (2012) 1785–1795.
- 674 [10] T. Friedrich, D. Scheide, The respiratory complex I of bacteria, archaea and eukarya
675 and its module common with membrane-bound multisubunit hydrogenases, *FEBS Lett.*
676 479 (2000) 1–5.
- 677 [11] R. Baradaran, J.M. Berrisford, G.S. Minhas, L.A. Sazanov, Crystal structure of the
678 entire respiratory complex I, *Nature* 494 (2013) 443–448.
- 679 [12] M. Horch, L. Lauterbach, M. Saggiu, P. Hildebrandt, F. Lenzian, R. Bittl, O. Lenz, I.
680 Zebger, Probing the active site of an O₂-tolerant NAD⁺-reducing [NiFe]-hydrogenase
681 from *Ralstonia eutropha* H16 by in situ EPR and FTIR spectroscopy, *Angew. Chem. Int.*
682 *Ed. Engl.* 49 (2010) 8026–8029.
- 683 [13] K. Karstens, S. Wahlefeld, M. Horch, M. Grunzel, L. Lauterbach, F. Lenzian, I.
684 Zebger, O. Lenz, Impact of the iron-sulfur cluster proximal to the active site on the
685 catalytic function of an O₂-tolerant NAD⁺-reducing [NiFe]-hydrogenase, *Biochemistry* 54
686 (2015) 389–403.
- 687 [14] K. Schneider, H.G. Schlegel, Production of superoxide radicals by soluble
688 hydrogenase from *Alcaligenes eutrophus* H16, *Biochem. J.* 193 (1981) 99–107.
- 689 [15] L. Lauterbach, O. Lenz, Catalytic production of hydrogen peroxide and water by
690 oxygen-tolerant [NiFe]-hydrogenase during H₂ cycling in the presence of O₂, *J. Am.*
691 *Chem. Soc.* 135 (2013) 17897–17905.
- 692 [16] T.H. Lonsdale, L. Lauterbach, S. Honda Malca, B.M. Nestl, B. Hauer, O. Lenz, H₂-
693 driven biotransformation of *n*-octane to 1-octanol by a recombinant *Pseudomonas putida*
694 strain co-synthesizing an O₂-tolerant hydrogenase and a P450 monooxygenase, *Chem.*
695 *Commun.* 51 (2015) 16173–16175.

- 696 [17] A.K. Holzer, K. Hiebler, F.G. Mutti, R.C. Simon, L. Lauterbach, O. Lenz, W. Kroutil,
697 Asymmetric biocatalytic amination of ketones at the expense of NH₃ and molecular
698 hydrogen, *Org. Lett.* 17 (2015) 2431–2433.
- 699 [18] H.A. Reeve, L. Lauterbach, P.A. Ash, O. Lenz, K.A. Vincent, A modular system for
700 regeneration of NAD cofactors using graphite particles modified with hydrogenase and
701 diaphorase moieties, *Chem. Commun. (Camb)* 48 (2011) 1589–1591.
- 702 [19] H.A. Reeve, L. Lauterbach, O. Lenz, K.A. Vincent, Enzyme-modified particles for
703 selective biocatalytic hydrogenation by hydrogen-driven NADH recycling,
704 *ChemCatChem* 7 (2015) 3480–3487.
- 705 [20] J. Ratzka, L. Lauterbach, O. Lenz, M.B. Ansorge-Schumacher, Systematic evaluation
706 of the dihydrogen-oxidising and NAD⁺-reducing soluble [NiFe]-hydrogenase from
707 *Ralstonia eutropha* H16 as a cofactor regeneration catalyst, *Biocatal. Biotransformation*
708 29 (2011) 246–252.
- 709 [21] N.R. Hayashi, T. Ishida, A. Yokota, T. Kodama, Y. Igarashi, *Hydrogenophilus*
710 *thermoluteolus* gen. nov., sp. nov., a thermophilic, facultatively chemolithoautotrophic,
711 hydrogen-oxidizing bacterium, *Int. J. Syst. Bacteriol.* 49 (1999) 783–786.
- 712 [22] E. Goto, T. Kodama, Y. Minoda, Growth and Taxonomy of Thermophilic Hydrogen
713 Bacteria, *Agric. Biol. Chem.* 42 (2014) 1305–1308.
- 714 [23] M. Taketa, H. Nakagawa, M. Habukawa, H. Osuka, K. Kihira, H. Komori, N. Shibata,
715 M. Ishii, Y. Igarashi, H. Nishihara, K.-S. Yoon, S. Ogo, Y. Shomura, Y. Higuchi,
716 Crystallization and preliminary X-ray analysis of the NAD⁺-reducing NiFe hydrogenase
717 from *Hydrogenophilus thermoluteolus* TH-1, *Acta Crystallogr. F Struct. Biol. Commun.*
718 71 (2015) 96–99.
- 719 [24] T. Burgdorf, E. van der Linden, M. Bernhard, Q.Y. Yin, J.W. Back, A.F. Hartog, A.O.
720 Muijsers, C.G. de Koster, S.P.J. Albracht, B. Friedrich, The soluble NAD⁺-reducing
721 NiFe-hydrogenase from *Ralstonia eutropha* H16 consists of six subunits and can be
722 specifically activated by NADPH, *J. Bacteriol.* 187 (2005) 3122–3132.
- 723 [25] T. Goris, A.F. Wait, M. Saggi, J. Fritsch, N. Heidary, M. Stein, I. Zebger, F.
724 Lenzian, F.A. Armstrong, B. Friedrich, O. Lenz, A unique iron-sulfur cluster is crucial
725 for oxygen tolerance of a [NiFe]-hydrogenase, *Nat. Chem. Biol.* 7 (2011) 310–318.
- 726 [26] J. Dervede, T. Eitinger, N. Patenge, B. Friedrich, *hyp* gene products in *Alcaligenes*
727 *eutrophus* are part of a hydrogenase-maturation system, *Eur. J. Biochem.* 235 (1996) 351–
728 358.
- 729 [27] I. Wolf, T. Buhrke, J. Dervede, A. Pohlmann, B. Friedrich, Duplication of *hyp* genes
730 involved in maturation of [NiFe] hydrogenases in *Alcaligenes eutrophus* H16, *Arch.*
731 *Microbiol.* 170 (1998) 451–459.
- 732 [28] I. Bürstel, E. Siebert, S. Frielingsdorf, I. Zebger, B. Friedrich, O. Lenz, CO
733 synthesized from the central one-carbon pool as source for the iron carbonyl in O₂-
734 tolerant NiFe-hydrogenase, *Proc. Natl. Acad. Sci. U. S. A.* 113 (2016) 14722–14726.
- 735 [29] K. Schneider, H.G. Schlegel, K. Jochim, Effect of nickel on activity and subunit
736 composition of purified hydrogenase from *Nocardia opaca* 1 b, *Eur. J. Biochem.* 138
737 (1984) 533–541.
- 738 [30] K. Schneider, H.G. Schlegel, Purification and properties of soluble hydrogenase from
739 *Alcaligenes eutrophus* H 16, *Biochim. Biophys. Acta* 452 (1976) 66–80.
- 740 [31] L. Lauterbach, Z. Idris, K.A. Vincent, O. Lenz, Catalytic properties of the isolated
741 diaphorase fragment of the NAD-reducing [NiFe]-hydrogenase from *Ralstonia eutropha*,
742 *PLoS One* 6 (2011) e25939.
- 743 [32] O. Schmitz, G. Boison, H. Salzmann, H. Bothe, K. Schutz, S.-h. Wang, T. Happe,
744 HoxE - a subunit specific for the pentameric bidirectional hydrogenase complex
745 (HoxEFUYH) of cyanobacteria, *Biochim. Biophys. Acta* 1554 (2002) 66–74.

- 746 [33] K. Ma, R. Weiss, M.W.W. Adams, Characterization of hydrogenase II from the
747 hyperthermophilic archaeon *Pyrococcus furiosus* and assessment of its role in sulfur
748 reduction, *J. Bacteriol.* 182 (2000) 1864–1871.
- 749 [34] L.T. Serebryakova, M. Medina, N.A. Zorin, I.N. Gogotov, R. Cammack, Reversible
750 hydrogenase of *Anabaena variabilis* ATCC 29413: catalytic properties and
751 characterization of redox centres, *FEBS Lett.* 383 (1996) 79–82.
- 752 [35] L. Cournac, G. Guedeney, G. Peltier, P.M. Vignais, Sustained photoevolution of
753 molecular hydrogen in a mutant of *Synechocystis* sp. strain PCC 6803 deficient in the type
754 I NADPH-dehydrogenase complex, *J. Bacteriol.* 186 (2004) 1737–1746.
- 755 [36] K. Gutekunst, X. Chen, K. Schreiber, U. Kaspar, S. Makam, J. Appel, The
756 bidirectional NiFe-hydrogenase in *Synechocystis* sp. PCC 6803 is reduced by flavodoxin
757 and ferredoxin and is essential under mixotrophic, nitrate-limiting conditions, *J. Biol.*
758 *Chem.* 289 (2014) 1930–1937.
- 759 [37] S.K. Chandrayan, P.M. McTernan, R.C. Hopkins, J. Sun, F.E. Jenney, M.W.W.
760 Adams, Engineering hyperthermophilic archaeon *Pyrococcus furiosus* to overproduce its
761 cytoplasmic NiFe-hydrogenase, *J. Biol. Chem.* 287 (2012) 3257–3264.
- 762 [38] K. Ma, R.N. Schicho, R.M. Kelly, M.W. Adams, Hydrogenase of the
763 hyperthermophile *Pyrococcus furiosus* is an elemental sulfur reductase or
764 sulfhydrogenase: evidence for a sulfur-reducing hydrogenase ancestor, *Proc. Natl. Acad.*
765 *Sci. U. S. A.* 90 (1993) 5341–5344.
- 766 [39] F.O. Bryant, M.W. Adams, Characterization of hydrogenase from the
767 hyperthermophilic archaeobacterium, *Pyrococcus furiosus*, *J. Biol. Chem.* 264 (1989)
768 5070–5079.
- 769 [40] F. Germer, I. Zebger, M. Saggi, F. Lendzian, R. Schulz, J. Appel, Overexpression,
770 isolation, and spectroscopic characterization of the bidirectional NiFe hydrogenase from
771 *Synechocystis* sp. PCC 6803, *J. Biol. Chem.* 284 (2009) 36462–36472.
- 772 [41] P. Kwan, C.L. McIntosh, D.P. Jennings, R.C. Hopkins, S.K. Chandrayan, C.-H. Wu,
773 M.W.W. Adams, A.K. Jones, The NiFe-hydrogenase of *Pyrococcus furiosus* exhibits a
774 new type of oxygen tolerance, *J. Am. Chem. Soc.* 137 (2015) 13556–13565.
- 775 [42] H. Ogata, T. Kramer, H. Wang, D. Schilter, V. Pelmeshnikov, M. van Gestel, F.
776 Neese, T.B. Rauchfuss, L.B. Gee, A.D. Scott, Y. Yoda, Y. Tanaka, W. Lubitz, S.P.
777 Cramer, Hydride bridge in NiFe-hydrogenase observed by nuclear resonance vibrational
778 spectroscopy, *Nat. Commun.* 6 (2015) 7890.
- 779 [43] L. Lauterbach, H. Wang, M. Horch, L.B. Gee, Y. Yoda, Y. Tanaka, I. Zebger, O.
780 Lenz, S.P. Cramer, Nuclear resonance vibrational spectroscopy reveals the FeS cluster
781 composition and active site vibrational properties of an O₂-tolerant NAD⁺-reducing
782 [NiFe] hydrogenase, *Chem. Sci.* 6 (2015) 1055–1060.
- 783 [44] Y. Xiao, M.-L. Tan, T. Ichiye, H. Wang, Y. Guo, M.C. Smith, J. Meyer, W. Sturhahn,
784 E.E. Alp, J. Zhao, Y. Yoda, S.P. Cramer, Dynamics of *Rhodobacter capsulatus* 2Fe-2S
785 ferredoxin VI and *Aquifex aeolicus* ferredoxin 5 via nuclear resonance vibrational
786 spectroscopy (NRVS) and resonance Raman spectroscopy, *Biochemistry* 47 (2008) 6612–
787 6627.
- 788 [45] D. Mitra, V. Pelmeshnikov, Y. Guo, D.A. Case, H. Wang, W. Dong, M.-L. Tan, T.
789 Ichiye, F.E. Jenney, M.W.W. Adams, Y. Yoda, J. Zhao, S.P. Cramer, Dynamics of the
790 4Fe-4S cluster in *Pyrococcus furiosus* D14C ferredoxin via nuclear resonance vibrational
791 and resonance Raman spectroscopies, force field simulations, and density functional
792 theory calculations, *Biochemistry* 50 (2011) 5220–5235.
- 793 [46] A. Volbeda, E. Garcin, C. Piras, A.L. DeLacey, V.M. Fernandez, E.C. Hatchikian, M.
794 Frey, J.C. Fontecilla-Camps, Structure of the [NiFe] hydrogenase active site: evidence for
795 biologically uncommon Fe ligands, *J. Am. Chem. Soc.* 118 (1996) 12989–12996.

- 796 [47] R.P. Happe, W. Roseboom, A.J. Pierik, S.P. Albracht, K.A. Bagley, Biological
797 activation of hydrogen, *Nature* 385 (1997) 126.
- 798 [48] K.A. Bagley, E.C. Duin, W. Roseboom, S.P.J. Albracht, W.H. Woodruff, Infrared-
799 detectable group senses changes in charge density on the nickel center in hydrogenase
800 from *Chromatium vinosum*, *Biochemistry* 34 (1995) 5527–5535.
- 801 [49] M.Y. Darensbourg, E.J. Lyon, J.J. Smee, The bio-organometallic chemistry of active
802 site iron in hydrogenases, *Coord. Chem. Rev.* 206-207 (2000) 533–561.
- 803 [50] M. Horch, L. Lauterbach, M.A. Mroginski, P. Hildebrandt, O. Lenz, I. Zebger,
804 Reversible active site sulfoxxygenation can explain the oxygen tolerance of a NAD⁺-
805 reducing [NiFe] hydrogenase and its unusual infrared spectroscopic properties, *J. Am.*
806 *Chem. Soc.* 137 (2015) 2555–2564.
- 807 [51] B.L. Greene, C.-H. Wu, P.M. McTernan, M.W.W. Adams, R.B. Dyer, Proton-coupled
808 electron transfer dynamics in the catalytic mechanism of a NiFe-hydrogenase, *J. Am.*
809 *Chem. Soc.* 137 (2015) 4558–4566.
- 810 [52] L. Lauterbach, J. Liu, M. Horch, P. Hummel, A. Schwarze, M. Haumann, K.A.
811 Vincent, O. Lenz, I. Zebger, The hydrogenase subcomplex of the NAD⁺-reducing [NiFe]
812 hydrogenase from *Ralstonia eutropha* - Insights into catalysis and redox interconversions,
813 *Eur. J. Inorg. Chem.* 2011 (2011) 1067–1079.
- 814 [53] R.P. Happe, W. Roseboom, G. Egert, C.G. Friedrich, C. Massanz, B. Friedrich, S.P.J.
815 Albracht, Unusual FTIR and EPR properties of the H₂-activating site of the cytoplasmic
816 NAD-reducing hydrogenase from *Ralstonia eutropha*, *FEBS Lett.* 466 (2000) 259–263.
- 817 [54] E. van der Linden, T. Burgdorf, M. Bernhard, B. Bleijlevens, B. Friedrich, S.P.
818 Albracht, The soluble [NiFe]-hydrogenase from *Ralstonia eutropha* contains four
819 cyanides in its active site, one of which is responsible for the insensitivity towards oxygen,
820 *J. Biol. Inorg. Chem.* 9 (2004) 616–626.
- 821 [55] S.T. Stripp, B. Soboh, U. Lindenstrauss, M. Braussemann, M. Herzberg, D.H. Nies,
822 R.G. Sawers, J. Heberle, HypD is the scaffold protein for Fe-(CN)₂CO cofactor assembly
823 in [NiFe]-hydrogenase maturation, *Biochemistry* 52 (2013) 3289–3296.
- 824 [56] M. Horch, P. Hildebrandt, I. Zebger, Concepts in bio-molecular spectroscopy:
825 vibrational case studies on metalloenzymes, *Phys. Chem. Chem. Phys.* 17 (2015) 18222–
826 18237.
- 827 [57] K. Schneider, R. Cammack, H.G. Schlegel, D.O. Hall, The iron-sulphur centres of
828 soluble hydrogenase from *Alcaligenes eutrophus*, *Biochim. Biophys. Acta* 578 (1979)
829 445–461.
- 830 [58] K. Schneider, R. Cammack, H.G. Schlegel, Content and localization of FMN, Fe-S
831 clusters and nickel in the NAD-linked hydrogenase of *Nocardia opaca* 1b, *Eur. J.*
832 *Biochem.* 142 (1984) 75–84.
- 833 [59] C. Zaborosch, M. Köstert, E. Bill, K. Schneider, H. Schlegel, A. Trautweint, EPR and
834 Mössbauer spectroscopic studies on the tetrameric, NAD-linked hydrogenase of *Nocardia*
835 *opaca* 1b and its two dimers: 1. The βδ-dimer - a prototype of a simple hydrogenase,
836 *Biometals* 8 (1995).
- 837 [60] A. Erkens, K. Schneider, A. Müller, The NAD-linked soluble hydrogenase from
838 *Alcaligenes eutrophus* H16: detection and characterization of EPR signals deriving from
839 nickel and flavin, *J. Biol. Inorg. Chem.* 1 (1996) 99–110.
- 840 [61] P.J. Silva, B. de Castro, W.R. Hagen, On the prosthetic groups of the NiFe
841 sulfhydrogenase from *Pyrococcus furiosus*: topology, structure, and temperature-
842 dependent redox chemistry, *J. Biol. Inorg. Chem.* 4 (1999) 284–291.
- 843 [62] J. Löwenstein, L. Lauterbach, C. Teutloff, O. Lenz, R. Bittl, Active site of the NAD⁺-
844 reducing hydrogenase from *Ralstonia eutropha* studied by EPR spectroscopy, *J. Phys.*
845 *Chem. B* 119 (2015) 13834–13841.

- 846 [63] R. Cammack, D.S. Patil, E. Hatchikian, V.M. Fernández, Nickel and iron-sulphur
847 centres in *Desulfovibrio gigas* hydrogenase: ESR spectra, redox properties and
848 interactions, *Biochim. Biophys. Acta.* 912 (1987) 98–109.
- 849 [64] B. Guigliarelli, C. More, A. Fournel, M. Asso, E.C. Hatchikian, R. Williams, R.
850 Cammack, P. Bertrand, Structural organization of the Ni and (4Fe-4S) centers in the
851 active form of *Desulfovibrio gigas* hydrogenase. Analysis of the magnetic interactions by
852 electron paramagnetic resonance spectroscopy, *Biochemistry* 34 (1995) 4781–4790.
- 853 [65] R.M. Kelly, J.W. Deming, Extremely thermophilic archaeobacteria: biological and
854 engineering considerations, *Biotechnol. Prog.* 4 (1988) 47–62.
- 855 [66] T. Reda, C.D. Barker, J. Hirst, Reduction of the iron-sulfur clusters in mitochondrial
856 NADH:ubiquinone oxidoreductase (complex I) by EuII-DTPA, a very low potential
857 reductant, *Biochemistry* 47 (2008) 8885–8893.
- 858 [67] T. Ohnishi, Iron–sulfur clusters/semiquinones in Complex I, *Biochim. Biophys. Acta*
859 1364 (1998) 186–206.
- 860 [68] E. Nakamaru-Ogiso, T. Yano, T. Yagi, T. Ohnishi, Characterization of the iron-sulfur
861 cluster N7 (N1c) in the subunit NuoG of the proton-translocating NADH-quinone
862 oxidoreductase from *Escherichia coli*, *J. Biol. Chem.* 280 (2005) 301–307.
- 863 [69] A. Porthun, M. Bernhard, B. Friedrich, Expression of a functional NAD-reducing
864 [NiFe] hydrogenase from the gram-positive *Rhodococcus opacus* in the gram-negative
865 *Ralstonia eutropha*, *Arch. Microbiol.* 177 (2002) 159–166.
- 866 [70] C.J. Marx, M.E. Lidstrom, Development of improved versatile broad-host-range
867 vectors for use in methylotrophs and other Gram-negative bacteria, *Microbiology* 147
868 (2001) 2065–2075.
- 869 [71] E. Schwartz, U. Gerischer, B. Friedrich, Transcriptional regulation of *Alcaligenes*
870 *eutrophus* hydrogenase genes, *J. Bacteriol.* 180 (1998) 3197–3204.
- 871 [72] L. Kleihues, O. Lenz, M. Bernhard, T. Buhrke, B. Friedrich, The H₂ sensor of
872 *Ralstonia eutropha* is a member of the subclass of regulatory [NiFe] hydrogenases, *J.*
873 *Bacteriol.* 182 (2000) 2716–2724.
- 874 [73] C. Massanz, S. Schmidt, B. Friedrich, Subforms and in vitro reconstitution of the
875 NAD-reducing hydrogenase of *Alcaligenes eutrophus*, *J. Bacteriol.* 180 (1998) 1023–
876 1029.
- 877 [74] U.K. Laemmli, Cleavage of structural proteins during the assembly of the head of
878 bacteriophage T4, *Nature* 227 (1970) 680–685.
- 879 [75] R. Wang, F.P. Healey, J. Myers, Amperometric measurement of hydrogen evolution
880 in *Chlamydomonas*, *Plant Physiol.* 48 (1971) 108–110.
- 881 [76] M. Neumann, G. Mittelstadt, F. Seduk, C. Iobbi-Nivol, S. Leimkuhler, MocA is a
882 specific cytidyltransferase involved in molybdopterin cytosine dinucleotide biosynthesis
883 in *Escherichia coli*, *J. Biol. Chem.* 284 (2009) 21891–21898.
- 884 [77] D. Moss, E. Nabedryk, J. Breton, W. Mäntele, Redox-linked conformational changes
885 in proteins detected by a combination of infrared spectroscopy and protein
886 electrochemistry. Evaluation of the technique with cytochrome *c*, *Eur. J. Biochem.* 187
887 (1990) 565–572.
- 888 [78] A.L. de Lacey, E.C. Hatchikian, A. Volbeda, M. Frey, J.C. Fontecilla-Camps, V.M.
889 Fernández, Infrared-spectroelectrochemical characterization of the [NiFe] hydrogenase of
890 *Desulfovibrio gigas*, *J. Am. Chem. Soc.* 119 (1997) 7181–7189.
- 891 [79] C. Fichtner, C. Laurich, E. Bothe, W. Lubitz, Spectroelectrochemical characterization
892 of the NiFe hydrogenase of *Desulfovibrio vulgaris* Miyazaki F, *Biochemistry* 45 (2006)
893 9706–9716.
- 894 [80] W. Sturhahn, CONUSS and PHOENIX: evaluation of nuclear resonant scattering data,
895 *Hyp. Interact.* 125 (2000) 149–172.

Supplementary Information

(supplementary figures S1-10)

```

HtHoxF 1 -----MTTERQ-RTAPGILAAIHQARSRFGRPLDAQALAEIISTAFSLPPGEIAATASFY
ReHoxF 1 MDSRITITILERYRSRDRTRIIDILWDVQHEYGHI-PDAVILPQLGAGLKLSPLDIRETASFY
TtNqo1 1 -----

HtHoxF 54 HFFQTP-PARYQIHFVDHVVVDHAGVAALCNHLCAAFATQPGQRTADARLFVGTACAGL
ReHoxF 60 HFFLDKPSGKYRIYLCNSVIAKINGYQAVREALERETGIRFGETDPNGMFGFLDTPCIGL
TtNqo1 1 -----

HtHoxF 113 SDQAPAAALINGRPMFRLDAARIDALIEKIQAQIPMDQ-----WPTWF-----AVTNAI
ReHoxF 120 SDQEPAMLLDKVVFTRLRPGKITDIIAQLKQGRSPAELIANPAGLPSQDIAYVDAMVESNV
TtNqo1 1 -----MTGPILSGLDPRFERTLYAHVKG

HtHoxF 162 HRHGPILLTWLDTTPAEAVFEHPTAHDPEDAILQAVTDAGLRGRGGAGFPATKWRFCRENA
ReHoxF 180 RTKGPVF-FRGRIDLRSLLDQCLLLKPEQVIETIVDSRLRGRGGAGFSTGLKWRLCRDAE
TtNqo1 33 EGSWTLDYLRHGGYETAKRVLKEKTPDEVIEEVKRSGLRGRGGAGFPGLKWSFMPKDD

HtHoxF 222 DPERFLICNADEGEPGTFKDRVLLTRYFEHLFAGMILAAARATGADKAILYLRYEYQYLLP
ReHoxF 239 SEQKYVICNADEGEPGTFKDRVLLTRAPKKVEVGMVIAAAYAICCRKGIYVLRGEYFYKLD
TtNqo1 84 GKQHYLICNADESEPGSEFKDRYIILEDVPHLLIBGMILAGYAIRATVGYIYVRGEYRRAAD

HtHoxF 282 QLEAARERIASA-----QATVPPAERVLTLEIALGAGAYVCGEESALIESLEKPKRPRVR
ReHoxF 299 YLERQLQELREDGLLGRAIGGRAGFDFDIRIQMGAGAYICGDESALIESCEGKRGTPRVK
TtNqo1 144 RLEQAIKEARARGYLGKNLFG-TDFSFDLHVHRGAGAYICGETALMNSLEGLRANPRLK

HtHoxF 337 PPFYVPTQGYLGHPTVNNVETLVAVAAATVGNAAWWRALGTPDSSGPKLFCVSGDVAQPG
ReHoxF 359 PFFFVQQGYLQKPTSVNNVETFAAVSRIMEEGADWFRAMGTPDSACTRLLSVAGDCSKPG
TtNqo1 203 PFFPAQSGLWQKPTTINNVELASVVEIMERGADWFAQMTEQSKGMKLYQISCPVKRPG

HtHoxF 397 LYEFYPCVALGDVVTA--ARPLGTRYAVQVSGPSGTLPLPATPEQLARPLAFEALPCNGT-
ReHoxF 419 IYEVVWCVTLNEVLAM--VGAR-DARAVQISGPGSECVSVA-KDGERKLAYEDLSCNGA-
TtNqo1 263 VYELPMGTTFRELIYEWAGGPLEPIQAIIPGSSTPPLPFTEEVLDTPMSYEHLLQAKGSM

HtHoxF 454 -----VMVFDVRRDPVAIVHHFARFEFAHESCGFCTPCRVTQQLI-AKTFEKIAAGYATRF
ReHoxF 474 -----FTIFNCKRDLEIVRDHMQFFVEESCGICVPCRAGNVDL-HRKVEWVIAGKACQK
TtNqo1 323 LGTGGVILIPERVSMVDAMWNLTRFYAHESCGKCTPCRECVAGFMVNLFAKIGTGQGEK

HtHoxF 508 DIERLAPALEAMRLASNCGFGLSAGNEVRDLIAHERQQLEAQLQPH--DFIPAFSLDAEL
ReHoxF 528 DLDDMVSWGALVVRTSRCGLCATSPKPIILTTLEKEPEIYQNKIVRHEGPLLPSFDLDTAL
TtNqo1 383 DVENLEALLPLIEGRSFCPLADAAVWPEVKGSLRHEKDQYLALAREKRPVPRPSLW--R--

HtHoxF 566 AATRRLTGRDDPHAHLAQFEQPEVTR
ReHoxF 588 GGYEKALK-----DLE-----EVTR
TtNqo1 -----

```

HtHoxF 1 -----MTTERQRTA-PGILAAIHQARSRFGRPLDAQALAEIISTAFSLPP
ReHoxF 1 -----MDSRITITILERYRSDRTRIIDILWDVQHEYCHIPDA-VLPQLGAGLKLSPP
TtNqO2 1 MGFFDDKQDFLEETFAYKYPPEGRRA--AIMPLLRRVQQUEEWIRPE-RIEEIARLVGTTTP

HtHoxF 44 GEIAATASFYHFFQ-TPPARYQIHFDVHVVDHHCVAALCNHCAAFAIQPCQRTADARL
ReHoxF 50 LDIRETASFYHFFLDKPSGKYRITLYLNSVIAKINCYQAVREALERETGIRFGETDPNGMF
TtNqO2 58 TEVMGVASFYSYQFVPTGKYHLQVCATLSCKLAGAEELWDYLTETLGIQPGEVTPDGLF

HtHoxF 103 FVGWTAACGLSDQAPAAALINGRPMPR-LDAARIDALIEKIQAQIPMDQWPTEWFAVTNAI
ReHoxF 110 GLFDTPCIGLSDQEPAMLIDKVVVETR-LRPGKITDIIAQLKQGRSPAIEIANPAGLPSQDI
TtNqO2 118 SVQKVECLGSCHTAPVIQVNDPEPYVECVTRARLEALLAGLRAGKRLEEIEELPGKCGH-HV

HtHoxF 162 HRHGPL
ReHoxF 169 AYVDAM
TtNqO2 177 HEVEV

HtHoxU 1 MRPTTPPFASETFTLDEESIPFVPGQTVLEAALAAAGRYIPLHLCWHPEMGNHGSRLCVVE
ReHoxU 1 -----MSIQITIDGKTLTTEEGRTLVDVAAENGVYIPLTLCYLKDKPCLGTCRVCSVK
TtNqo3 1 -----MVRVKVNDRIVEVPECTSVMDAVFHAGYDVPFLFCSEKHLSPICACRMCLVR

HtHoxU 61 AN-----GRIQASCALPAQFGLOVSKSETLTRVVRTLLEML
ReHoxU 53 VN-----GNVAAACTVRVSKGINVEVNDPELVDMRKALVEFL
TtNqo3 52 IGLPKKGPDPGKPLLNEKGEPEIQWQPKLAASCVTAVADGMVVDTLSDVVREAQAGMVEFT

HtHoxU 98 FAEGNHFCPGCEKSGDCLLQALAYAHGMTASHED-----PFYPPORRIDA---SH
ReHoxU 90 FAEGNHNCPSCEKSGRCQLQAVGYEVDMMVSRFP-----YRFVVRVDH---AS
TtNqo3 112 LLNHPLDCPTCDKGGACELQDRTVEYGLYEKYYQKGPLELVPYTRFEFTRRHVDKHHPLS

HtHoxU 144 PDLWLDPNRCILCGLCVRASL--AEGKEALVTGGRGIASRLLATSASGRLGDTALAATDR
ReHoxU 136 EKIWLERDRCIFCQRCVEFIRDKASGRKIFSTSHRGPESRIEIDAELA--NAMPPEQVKE
TtNqo3 172 PFVILLDRERCIHCRCVRYFEE-VPGDEVLDVFIERGVHTFIGTMD-----FGLPSGFSGN

HtHoxU 202 AARICPVGALNFKAAGFTTPIGKRRFDHRPPEAMSDKERYT-----
ReHoxU 194 AVAICPVGITILEKRVGYDDPIGRRKYEIQSVRARALEGEDK-----
TtNqo3 226 ITDICPVGALLDLTARFRA----RNWEMEETPTTCALCPVGGGITADTRSGELLRIRARE

HtHoxY 1 -----MTSAAPSAMPPrKIRIATASLAGCFGHMSFADIDTRI
ReHoxY 1 --MRA---PHKDEIASHELDPATPMDPALAANREGKIKVATIGLCGCWGC TLSFLDMDERL
TtNqo6 1 MALKDLFERDVQELEREGILFTTLEKLVAVGRSNSLWPAATFGLACCAIEMMASTDARNDL

HtHoxY 39 LALAIEWVTFRSPLTDWKTIV-GECDIALIEGGVCNAENVEVIRAY--RRAARILVAVGAC
ReHoxY 56 LPLLEKVTLLRSSLTDIKRIPERCATGFVEGGVSSBENIETLEHF--RENCNILISVGAC
TtNqo6 61 -----ARFGSEVFRASPRQADVMIVACRLSKKMAPVMRRVWEQMPDPKQWVISMGAC

HtHoxY 96 AINGGLPAQRNQHRVERLLTQVFEADRHLAPGS--RVNDPELPLLEHHPHIEITVRVD
ReHoxY 114 AVWGGVPAMRNVFELKDCLAEAYVNSATAVPGAKAVVPHFDIPRITTKYVPCHEVVKMD
TtNqo6 112 ASSGGMFNN-----YATVQNVDSVVPVD

HtHoxY 154 YYLPGCPPTAEVITWFTLTDLL---VCREP-----HFYPTLRYD----
ReHoxY 174 YFIPGCPPDGDAIFKVLDDLV---NCRPF-----DISSINRYD----
TtNqo6 135 VYVPGCPPRPEALIIYAVMQLQKKVRCQAYNERGERLEP-VAAWKRTRG

HtHoxH 1 ----MTQHAPQAVSPRPSLPA-NATRRVAID~~ELSR~~VEGHGKVTIWLDDDG-QVVEARLHI
ReHoxH 1 -----MSRKLVID~~EVTR~~IEGHGKVVVHLDDDN-KVVDAKLHV
TtNqo4 1 MREEFLEEIPLDAPPEEAKELRTEVMTLNVG~~EQ~~-HPSTHG~~VLR~~LRMLMVTLSGEEVLEVVPHI

HtHoxH 55 -VEFRGFEAFIVGRPYWEAPVVVOR~~LCGIC~~FPVSHH~~LAAAKALDRL~~VGVT-----QLPPTA
ReHoxH 37 -VEFRGFEKEFVQGHPEFWEAPMFLOR~~ICGIC~~FPVSHH~~CGAKALDDM~~VGVLKSGIHVTPTA
TtNqo4 60 GYLHTGFEKTMEHRTYLQNIITYTFR~~MDYLHSFAHDL~~AYALAVEKLLGA-----VVPRA

HtHoxH 109 EKMRRLMHYGQV~~LQSH~~ALHFFYL~~AAPD~~LL~~CF~~SADPAQRNVFGLAAQKRE~~LARQ~~GILVRQ
ReHoxH 96 EKMRRLGHYAQM~~LQSH~~TTAYFYLLIVPEM~~LF~~GM~~DAP~~PAQRNVLGLIEANPD~~L~~VKRVM~~L~~RK
TtNqo4 114 ETIRVILNELSRI~~LASH~~L---VFL~~GT~~GLLDL~~CG~~ALTPF-----FYAFRE-----RE

HtHoxH 169 FGQECIEATAGKRIHGTSAVP~~GGI~~HKNLSR~~RE~~RMALLSRAPEIRSW--CEAAVALIERLF
ReHoxH 156 WGQEVIKAVFGK~~KMHG~~INSVP~~GGV~~VNNLSIAERDRFLNGEGLLSVDQVIDYAQDGLRLF
TtNqo4 155 TILDLFEWVTGQR~~FHHNY~~IRI~~GG~~VKEDLPEEFVPELKKLLE-----VLPHRIDEY

HtHoxH 223 TE---HAPFFAQ~~GS~~FQTKTFS~~LVA~~ADGSLDLYD~~CT~~FRVKEANGAILIDHYDPNDYDQL
ReHoxH 216 YDFHQKHRAQVDSE~~AD~~VPALSMCLV~~GDD~~NDVDYH~~CR~~LRIIDDDKH-IVREFDYHDYLDH
TtNqo4 205 EALFAESPIFYERARGVGVIPPE---VAIDLGLT~~GS~~LRASGVNYD-VRKAYPYSGYETY

HtHoxH 283 LVEAVRPWSYMK~~F~~PYLKAYGE~~PD~~GFYRVG~~PS~~ARLINC~~DR~~LTTARAEARQR~~FL~~TFDQ~~G~~TV
ReHoxH 275 FSEAVEEWSYMK~~F~~PYLKELGREQGS~~V~~RVG~~PL~~GRMNVTKSLPTPLAQEALERFHAYTKGRT
TtNqo4 259 TFDVPLGERGDV~~F~~DRM-----

HtHoxH 343 AHS~~TL~~GYHWAR~~L~~IEM~~LH~~CAELIEAL~~L~~TD---AD~~LE~~GGEL~~R~~AR---GQRQHRG~~V~~G-----
ReHoxH 335 NNM~~TL~~H~~TN~~WAR~~A~~EIL~~H~~AAEVV~~KEL~~LHD---PDL~~Q~~KDQ~~L~~VLTPPPNAWTGEG~~V~~G-----
TtNqo4 277 -----LV~~R~~IRE~~M~~RESVKIIKQAL~~ER~~LEPGPVRDPNPQITPPPRHLETSM~~E~~AVIYHF

HtHoxH 391 -----VIE~~AP~~R~~G~~TL~~L~~H~~H~~YEVGDDDLITYCN~~L~~IVS~~T~~TH~~N~~NAV~~M~~NQAVTTA
ReHoxH 386 -----VVE~~AP~~R~~G~~TL~~L~~H~~H~~YRADERGNI~~T~~FAN~~L~~V~~A~~TTON~~N~~QVM~~N~~RTVRSV
TtNqo4 329 KHYTEGFHPPKGEVYVPT~~ES~~ARGE-~~L~~GY~~Y~~IVSDGGSMPYRVKVRAP-----

HtHoxH 435 AKAF~~LS~~GV-TL~~TE~~ALLN~~H~~IEVAVRA~~F~~DP~~CL~~SCATHALGOM~~PL~~VVS~~L~~HHKDVPT~~P~~ID~~M~~LVR
ReHoxH 430 AEDYL~~GG~~HGEITE~~G~~M~~N~~AIEV~~G~~IRAY~~DP~~CL~~SC~~ATHALGOM~~PL~~VVS~~V~~FDAAGRL-IDERAR
TtNqo4 374 --S~~F~~VN~~L~~Q-----SLPY~~AC~~KGEQVPDMVAIIASLDPV~~M~~GDVD-----

HtHoxH 494 HSDGTIERPTAAPALGTKGT
ReHoxH 489 -----
TtNqo4 404 -----

```

HtHoxW      1  --MTTQYPERPILLPAPPPPGAILLACGNDLRGDDALGARFVAETIERQKQTLPPAWRDAI
ReHoxW      1  MNAPAEFFPYVTLADF--DDPSTLIYGICNVGRQDDGLGWAFIDRLEAESLCSG----AEV

HtHoxW     59  VTHWQLQWGPETALLLANRHTVCFVDAYAPNGIEASPHGAERAAAPFVVTLEPPDGTL
ReHoxW     55  QRHYQLHL--EDADLISRKRKVLFI DATK DASV-----ASFSLERAEP RMD F-

HtHoxW    119  APLLASVGT HQVSP IALLAAARLLGLALPASLWQIATRGEHFTLGAPLSALASRA LAETL
ReHoxW    100  -----SFTSHAISIPSIMATCQ-RCFQCLPEVYVLAIRGYEWELRMGLTPQARHNLDDAI

HtHoxW    179  TWFWPWLVGETIP ICTNGTITLN
ReHoxW    154  AHESMRAERQTS-----

```

Fig. S1. Alignments of the *Ht*SH subunits, HoxF, U, Y, and H, with those of *Re*SH, and the corresponding Nqo1/2, 3, 6, and 4 subunits of Complex I from *Thermus thermophilus* (*Tt*). Also given is the alignment of the SH-specific endopedidases (HoxW) of *Ht* and *Re*. Amino acid residues that are conserved in all three species are highlighted in red, those conserved only among *Ht* and *Re* are boxed in black. Amino acid residues supposed to be involved in the coordination of Fe-S clusters are indicated in green, those involved in the coordination of the NiFe catalytic center are shown in blue. HoxF represents a fusion protein of Nqo2 and Nqo1 from *Tt*. Therefore, two separate alignments were made. One shows the alignment of the complete *Ht* and *Re* HoxF proteins with Nqo1 (revealing similarities in a large C-terminal region), and the other one aligns the N termini of the two HoxF proteins with Nqo2. The Nqo3 subunit of *Thermus thermophilus* consists of 783 amino acid residues. As the HoxU subunits of *Ht* and *Re* represent a truncated form of Nqo3, only the first 281 amino acid residues of Nqo3 were used for the alignment.

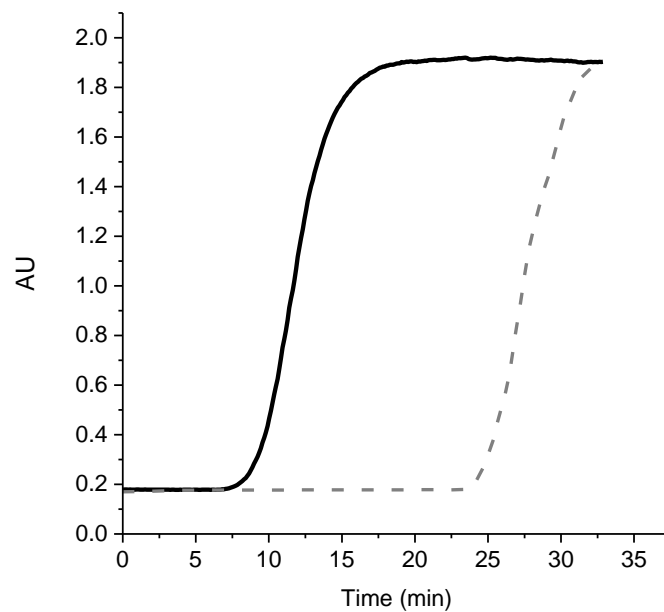


Fig. S2. Kinetics of H₂-dependent NAD⁺-reduction (given in absorption units, AU, at 365 nm) catalyzed by *Ht*SH with (solid line) and without (dashed line) the addition of FMN (2 μM). The assay was performed with 0.5 μM *Ht*SH at 50 °C in 50 mM bis-Tris, pH 6.5, supplemented with 1 mM NAD⁺, 0.5 mM NiCl₂, 5 mM MgSO₄, and 0.75 mM TCEP.

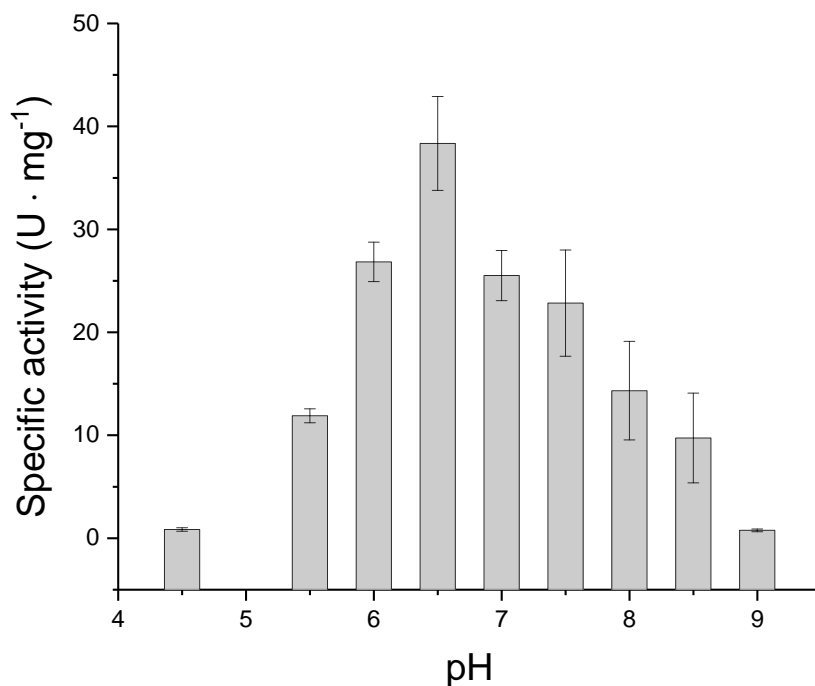


Fig. S3. pH dependence of the H₂-dependent NAD⁺ reduction activity of purified *Ht*SH protein on different pH values. The assay contained 60 nM *Ht*SH in one of the following buffers: pH 4.5–7.0, 50 mM citrate; pH 7.5–8.0, 50 mM Tris/HCl; pH 8.5–9.0, 50 mM glycine. Activity was measured in the presence of 1 mM NAD⁺, 0.5 mM NiCl₂, 5 mM MgSO₄, 2 μM FMN, and 0.75 mM TCEP at a temperature of 50 °C.

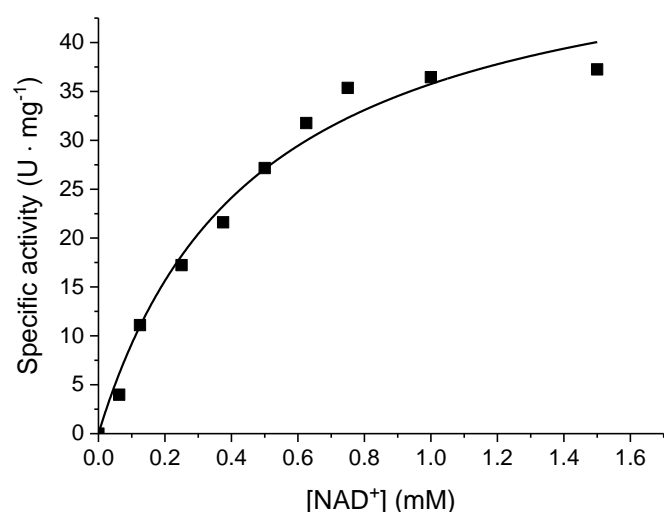


Fig. S4. Determination of the $K_M^{\text{NAD}^+}$ by measuring *HtSH*-mediated H_2 oxidation at different NAD^+ concentrations. Activity was measured at a temperature of 50 °C in 50 mM H_2 -saturated bis-Tris buffer, pH 6.5, 0.125–1.5 mM NAD^+ , 0.5 mM NiCl_2 , 5 mM MgSO_4 , 2 μM FMN, and 0.75 mM TCEP. The depicted values (squares) represent the means derived from at least two measurements of one protein preparation. The Michaelis-Menten constant and the corresponding v_{max} value were calculated by non-linear regression. From three biological replicates, a K_M of 469 μM with a coefficient of variation (CV) of 9.8 % was derived. The v_{max} value was 52.7 U mg^{-1} , with a CV of 3.4 %, resulting in a turnover frequency (k_{cat}) of $(155 \pm 5) \text{ s}^{-1}$ (assuming a molecular weight of 167.8 kDa for the heterotetrameric *HtSH*).

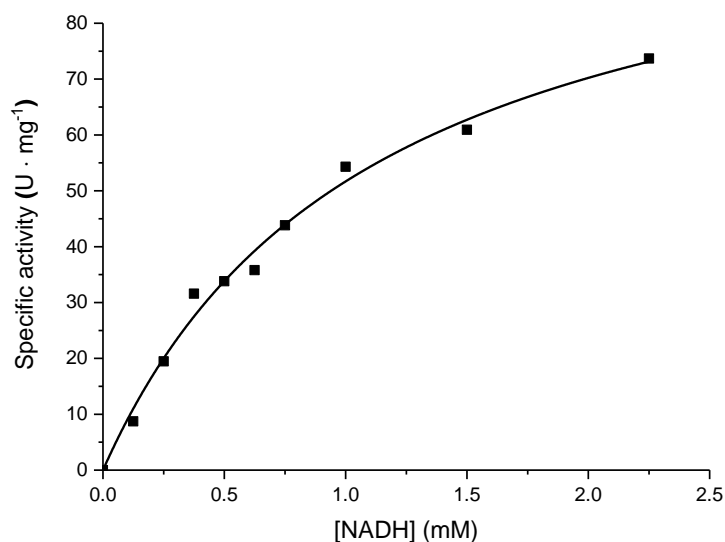


Fig. S5. Determination of the K_M^{NADH} by measuring the *HtSH*-mediated benzyl viologen reduction activity (squares) at different NADH concentrations. Activity was measured at a temperature of 50 °C in 50 mM bis-Tris buffer, pH 6.5, containing 5 mM benzyl viologen, 0.125–2.25 mM NADH , 0.5 mM NiCl_2 , 5 mM MgSO_4 , 2 μM FMN, and 0.75 mM TCEP. The Michaelis-Menten constant and the corresponding v_{max} value were calculated by non-linear regression. From two biological replicates, a K_M of 1.17 mM with a CV of 4.8% was derived. The v_{max} value was 64.9 U mg^{-1} , with a CV of 3.5 %, resulting in a turnover frequency (k_{cat}) of $(179 \pm 6) \text{ s}^{-1}$ (assuming a molecular weight of 167.8 kDa for the heterotetrameric *HtSH*).

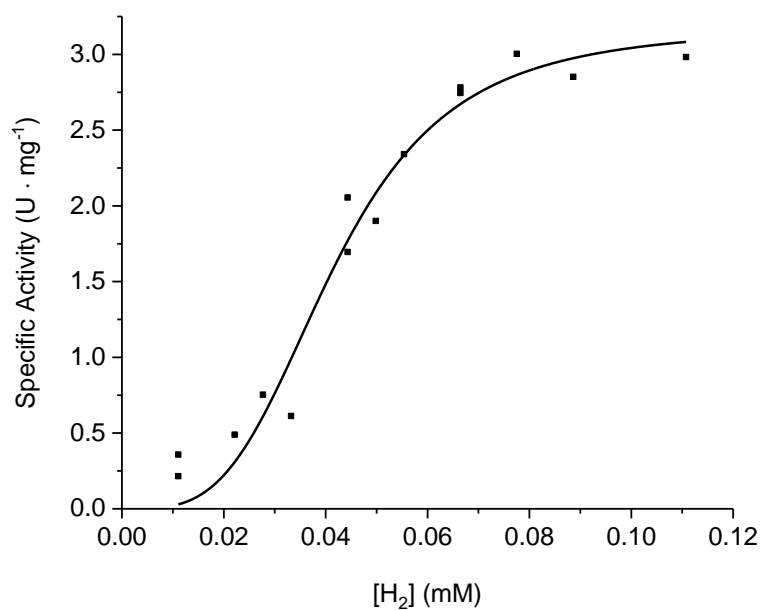


Fig. S6. Determination of the K_M^{app} for H_2 by measuring *Ht*SH-mediated NAD^+ reduction (squares) at different H_2 concentrations. Activity was measured at a temperature of 50 °C in 50 mM bis-Tris buffer, pH 6.5, containing 1 mM NAD^+ , 0.5 mM NiCl_2 , 5 mM MgSO_4 , 2 μM FMN, and 0.75 mM TCEP. The resulting data were not compatible with a classical Michaelis-Menten fit. Therefore, the K_M^{app} for H_2 (ligand concentration, at which half the ligand-binding sites are occupied) was calculated by non-linear regression ($R^2 = 0.959$) and revealed to be $41.6 \pm 2.5 \mu\text{M}$ with a Hill coefficient of 2.87 ± 0.8 . The origin of the apparent cooperativity is unclear.

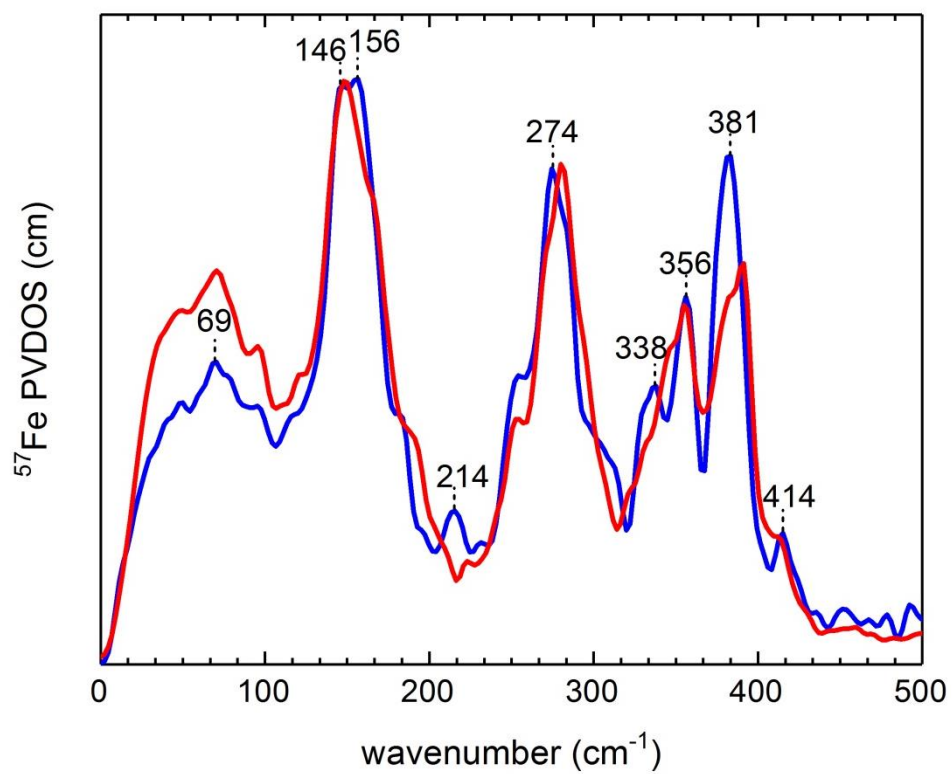


Fig. S7. NRVS-derived ^{57}Fe PVDOS in the spectral region reflecting Fe-S cluster modes. The spectra of as-isolated, oxidized *HtSH* and *ReSH* (the latter was taken from reference [43]) are shown as blue and red traces, respectively.

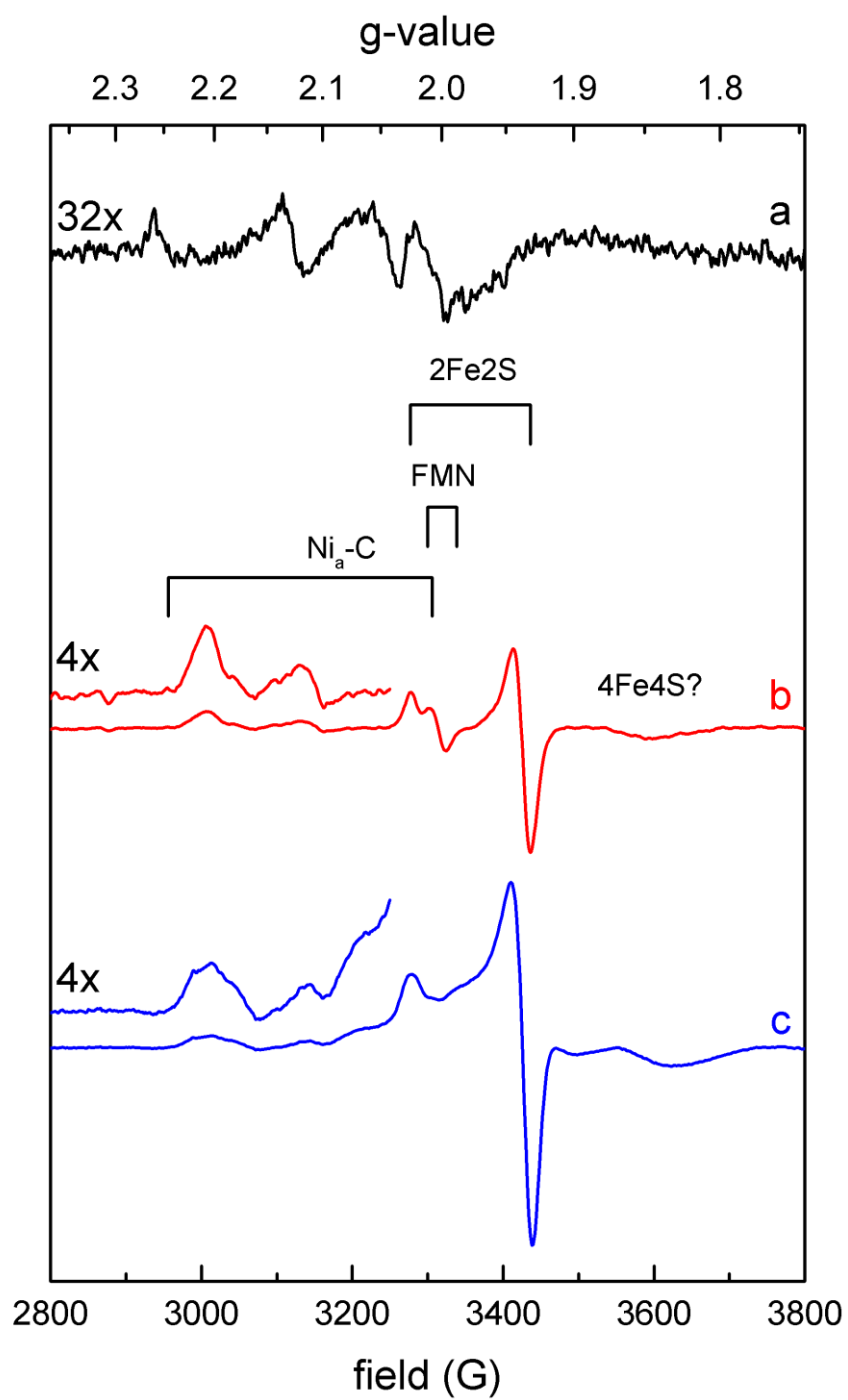


Fig. S8. EPR spectra of (a) as-isolated, (b) TCEP/NADH-reduced and (c) TCEP/NADH/H₂-reduced *HtSH*. Spectra were recorded at 35 K (a), 10 K (b), and 6.5 K (c).

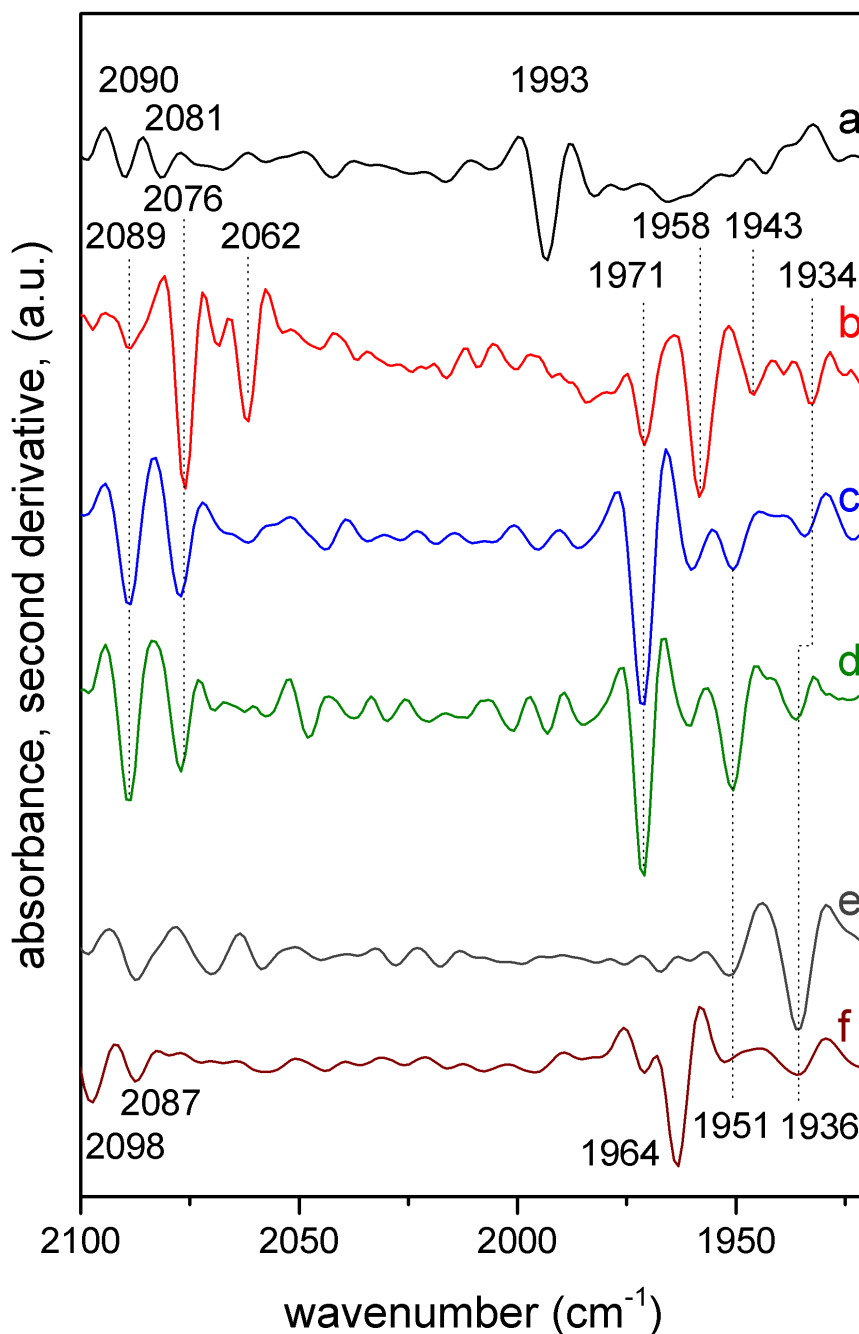


Fig. S9. IR spectra of *HtSH* from spectro-electrochemical measurements. Spectra were recorded at a) open circuit potential (+270 mV), b) -440 mV, c) -350 mV, d) -310 mV, e) -190 mV, and f) +460 mV vs. SHE. The spectro-electrochemical data essentially confirm the band assignments made above, and the enrichment of Ni_r-S is found to require higher potentials than the formation of Ni_a-S (traces d and e). Moreover, CN stretching frequencies of Ni_a-S, Ni_r-B-like, and the 1993 cm⁻¹ species can be tentatively assigned to signals at 2089/2076, 2098/2087, and 2090/2081 cm⁻¹, respectively (traces a, d, and f). While CN stretching bands of Ni_r-S cannot be clearly identified in the spectro-electrochemical data (trace e), the entirety of all previous assignments leaves the two bands at 2071 and 2058 cm⁻¹ (Fig. 6, traces a and b) as the most plausible candidates.

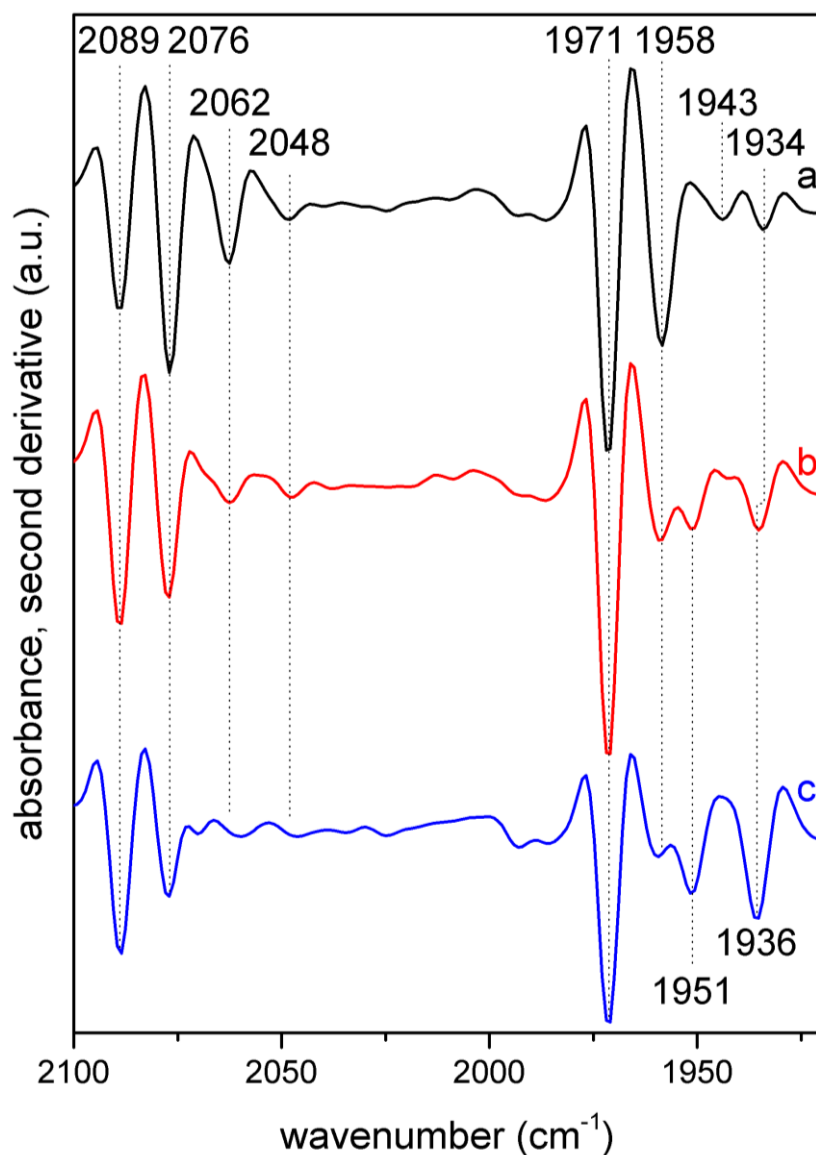


Fig. S10. IR spectra of TCEP/NADH/H₂-treated *HtSH*, recorded at 10 °C after slow re-oxidation of the enzyme, achieved by diffusion of air for 0.5 h (a), 5 h (b), and 8 h (c) into the IR cell. Trace a represents the spectrum of *HtSH* recorded directly after hydrogen incubation (analogous to Fig. 6, trace c). After approximately 5 h, intensities of the bands at 1934, 1943, and especially 1958 cm⁻¹ decreased in favor of the signals at 1971 and 1951 cm⁻¹ (trace b), which indicates conversion of the fully reduced states to Ni_a-C (and Ni_a-S). Consistently, the intensity of CN stretching bands assigned to Ni_a-SR (2076 and 2062 cm⁻¹) decreased as well, revealing a faint doublet at ca. 2062 and 2048 cm⁻¹, which may reflect residual amounts of the Ni_a-SR' and/or Ni_a-SR'' subspecies [12,50]. Upon further re-oxidation (8 h of air diffusion into the IR cell, trace c), the band at 1936 cm⁻¹ re-appeared, and the signal at 1951 cm⁻¹ increased in intensity. The obtained spectrum resembles the one recorded from the TCEP/NADH-reduced sample, reflecting conversion of Ni_a-C into Ni_r-S and Ni_a-S (Fig. 6 trace c). Thus, findings from slow re-oxidation experiments support the IR assignment of typical [NiFe] species detected for *HtSH* and their interrelations.